

# Mechanically and Chemically Robust Serum Albumin Hydrogels for Drug Delivery

## Dissertation

zur Erlangung des Doktorgrades der Naturwissenschaften  
(Dr. rer. nat.)

der

Naturwissenschaftlichen Fakultät II  
Chemie, Physik und Mathematik

der Martin-Luther-Universität  
Halle-Wittenberg

vorgelegt von

Frau Niuosha Sanaeifar



**First Reviewer**

Prof. Dr. Dariush Hinderberger  
MLU Halle-Wittenberg  
Institute of Physical Chemistry  
Von-Danckelmann-Platz 4  
06120 Halle (Saale)  
Germany

**Second Reviewer**

Prof. Dr. Annette M. Schmidt  
University of Cologne  
Department of Chemistry  
Greinstraße 4-6  
50939 Cologne  
Germany

Date of public defense: 13.06.2024

I declare in lieu of an oath that I have written this cumulative PhD thesis independently and exclusively using the indicated aids and sources.

All text passages that are taken verbatim or in terms of content from publications have been marked as such.

Furthermore, I assured that I have not submitted this work to any other institution.

I am aware that if I make false statements, I will be deemed to have failed the examination and I assure with my signature the correctness of this information. I acknowledge all legal principles.

---

Niuosha Sanaeifar

30.06.2022

---

Date

## **Abstract**

The purpose of this thesis was to develop a controlled release system based on bovine serum albumin (BSA) hydrogels. To achieve this goal, hydrogels from BSA were prepared by thermally, pH or ethanol induced procedures to study the release behavior of a model “drug” 16-doxy stearic acid, spin-labeled coumarin-3-carboxylic acid, warfarin and naproxen. The macroscopic properties of these gels were studied through rheology, while the secondary structure changes of the protein were analyzed via infrared (IR) spectroscopy. The combined effects of type of drug, drug concentration, duration of gel formation, and gelation methods on release behavior were characterized by continuous wave electron paramagnetic resonance (CW EPR) spectroscopy and dynamic light scattering (DLS).

**Keywords:** albumin; hydrogel; EPR spectroscopy; release behavior; fatty acid; spin-labeled pharmaceutical

## Kurzdarstellung

Ziel dieser Arbeit war es, ein System zur kontrollierten Freisetzung zu entwickeln, das auf Rinderserumalbumin (BSA)-Hydrogelen basiert. Um dieses Ziel zu erreichen, wurden Hydrogele aus BSA durch thermische, pH oder Ethanol induzierte Verfahren hergestellt, um das Freisetzungsverhalten eines Modell-"Medikaments" 16-Doxyl-Stearinsäure, spin-markierte Cumarin-3-Carbonsäure, Warfarin und Naproxen zu untersuchen. Die Gelbildung wurde mithilfe von Rheologie makroskopisch untersucht, während die Sekundärstrukturänderungen des Proteins durch Infrarotspektroskopie (IR) analysiert wurden. Die kombinierten Auswirkungen der Art des Arzneimittels, der Arzneimittelkonzentration, der Dauer der Gelbildung und der Gelierungsmethoden auf das Freisetzungsverhalten wurden mit Hilfe der CW-EPR-Spektroskopie (Continuous Wave Electron Paramagnetic Resonance) und der dynamischen Lichtstreuung (DLS) charakterisiert.

**Stichworte:** Albumin; Hydrogel; EPR-Spektroskopie; Freisetzungsverhalten; Fettsäure; spin-markiertes Arzneimittel

## Table of Contents

1	Publication List .....	1
2	Introduction.....	2
3	Theory and Methods.....	12
3.1	Rheology .....	12
3.2	ATR-IR spectroscopy .....	15
3.3	Continuous Wave Electron Paramagnetic Resonance (CW EPR) Spectroscopy.....	16
3.4	Dynamic Light Scattering (DLS) .....	23
4	Results .....	26
4.1	Overview over the publications .....	26
4.1.1	Nanoscopic characterization of stearic acid release from bovine serum albumin hydrogels .....	26
4.1.2	Molecular-level release of coumarin-3-carboxylic acid and warfarin-derivatives from BSA-based hydrogels.....	28
4.1.3	Macro- and nanoscale effect of ethanol on bovine serum albumin gelation and naproxen release .....	29
4.2	Publications .....	30
5	Discussion .....	83
6	Conclusions and Outlook.....	91
7	References .....	94
8	List of Abbreviations and Symbols.....	100
8.1	Abbreviations .....	100
8.2	Symbols .....	101
9	Acknowledgments .....	103
10	Academic Curriculum Vitae .....	104

# 1 Publication List

P1. Sanaeifar N, Mäder K, Hinderberger D

**Nanoscopic characterization of stearic acid release from bovine serum albumin hydrogels**

Macromolecular Bioscience. 20(8), 2000126 (2020).

P2. Sanaeifar N, Mäder K, Hinderberger D

**Molecular-level release of coumarin-3-carboxylic acid and warfarin-derivatives from BSA-based hydrogels**

Pharmaceutics. 13(10), 1661 (2021).

P3. Sanaeifar N, Mäder K, Hinderberger D

**Macro- and nanoscale effect of ethanol on bovine serum albumin gelation and naproxen release**

International Journal of Molecular Sciences. 23(13), 7352 (2022).

For the mentioned publications, I planned and conducted all experimental works. I prepared samples and performed different characterization techniques, namely rheology, ATR-IR spectroscopy, CW ERP spectroscopy, EPRI and DLS. After accurate data evaluation, I wrote and prepared manuscripts which were reviewed by Prof. Dr. Dariush Hinderberger and Prof. Dr. Karsten Mäder. D. Hinderberger supervised the whole research.



## 2 Introduction

A wide variety of therapeutic drugs have been discovered and developed to treat severe diseases. However, nonspecific biodistribution and rapid consumption by the system result in low drug efficacy and undesirable therapeutic activity. Furthermore, due to low water solubility and cellular uptake of some therapeutic agents, more amount of drug is required to maintain the desired plasma level. Therefore, frequent dosing is needed which results in acute side effects and more discomfort to patients. The nature of the drug and administration route can be the reasons of this uneven behavior [1-3]. To address these challenges, various drug delivery and drug targeting systems have received tremendous attention from pharmaceutical industries worldwide [2, 4]. Since this research topic is of immense importance, drug delivery systems based on bovine serum albumin (BSA) hydrogels are developed and release of different pharmaceuticals are studied in this dissertation.

Great effort has been devoted to develop controlled drug delivery systems which can provide several advantages over traditional pharmaceutical formulations [5, 6]. These systems are designed to deliver drugs at predetermined rates and preferably for an extended period of time to provide an appropriate drug concentration for its optimum therapeutic activity [3, 6]. For this purpose, first, an active agent is partly released from a controlled delivery system to reach rapidly the effective therapeutic concentration. Subsequently, drug release kinetics follow a well-defined behavior to control drug concentration in blood plasma [4]. Figure 2.1 shows the schematic of a controlled drug delivery system. The administration of drugs by a drug delivery system can diminish harmful side effects since the drug is delivered locally rather than systematically, which can enhance patient compliance [7].

Despite many advantages of a controlled drug delivery system, it is important not to ignore the potential disadvantages such as the possible toxicity or non-biocompatibility of materials used, undesirable byproducts of degradation, necessary surgery for implantation or removing of the system and higher cost in comparison with conventional drug formulations [8].

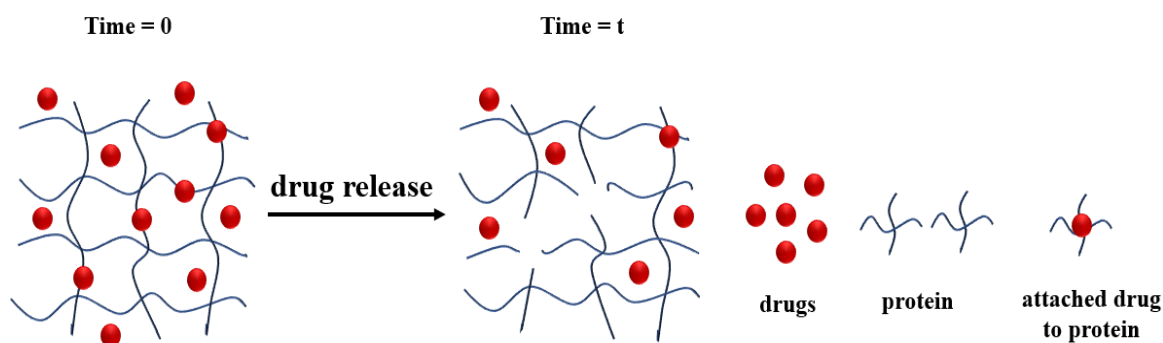


Figure 2.1 Schematic representation of a controlled drug delivery system.

It is important to mention that different parameters such as temperature, pH, surfactant, agitation rate, and presence of enzymes can affect drug release rate. For example, increasing temperature can improve hydration and degradation of polymeric carriers, which leads to higher drug release rate. Moreover, accelerated drug release from biodegradable polyesters can be obtained by both acidic and basic conditions. Addition of surfactant or organic solvents into the release medium can hasten drug release. For example, when faster drug release from lipid implants is desirable, the addition of surfactant in the release medium can facilitate wetting and buffer diffusion into the system, which can increase drug solubility and release rate [9].

Numerous systems have been tried as vehicles of controlled drug delivery such as nanocarriers [10, 11], polylactic acid (PLA) and poly(lactic-co-glycolic acid) (PLGA) products [12, 13], smart polymers [14, 15], hydroxyapatite (HA) [16], hydrogels [17-19], and others.

Considerable interest has been shown in the use of hydrogels as a carrier for controlled drug delivery systems. Hydrogels are crosslinked networks made from hydrophilic polymers, proteins or small molecules with the capability of absorbing water from 10-20 percent up to thousands times of their own weight, due to the presence of physical and chemical bonds within polymeric network. Their high water content resembles living tissue and minimizes negative immune reaction after implantation. Due to this property, hydrophilic drugs can be incorporated in the water-swollen network of hydrogels. There is low probability of drug degradation and aggregation upon exposure to organic solvents, since hydrogels may provide desirable protection [20-23].

Natural proteins have gained significant interest in recent years to be used as a carrier for drug delivery applications [6]. In the three publications presented in

this thesis, bovine serum albumin (BSA) was selected as a drug carrier to develop a novel drug delivery vehicle. As a major protein in blood plasma, albumin is responsible for maintaining colloid osmotic pressure and reversible binding to a wide variety of substances such as hormones, fatty acids, drugs and polypeptides through the blood stream. This 66 kDa monomer protein contains multiple hydrophobic binding pockets and plays a significant role in transportation and deposition of different categories of molecules to different tissues through physical or chemical bonding to the binding sites of this protein [24, 25]. Serum albumin, a small globular and in the crystalline state heart-shaped molecule, consists of 607 amino acids with an isoelectric point of 4.7 in water at 25 °C [26, 27]. Moreover, the negatively charged surface makes albumin highly water soluble [28]. Due to its low toxicity and immunogenicity, high biocompatibility, biodegradability, and considerable ligand-binding characteristics, albumin is being evaluated in many drug delivery applications [27].

Structurally, albumin consists of three homologous domains I, II, and III, connected by random coil and each domain has two long and one shorter loops. The first two loops in each domain form subdomain A and the last loop in each domain is denoted as subdomain B. Subdomains A and B contain 4 and 6  $\alpha$ -helices, respectively [24, 29]. Although, the domains are similar in structure, their ligand-binding affinities and functions are found to be different. Two main drug binding sites in albumin are denoted as Sudlow site I and Sudlow site II. They are positioned in the hydrophobic cavities of subdomains IIA and IIIA, respectively. It has been found that large heterocyclic and negatively charged compounds such as azapropazone, phentylbutazone and warfarin bind with high affinity to Sudlow site I, while Sudlow site II prefers small aromatic carboxylic acids like ibuprofen [24, 25, 28]. Figure 2.2 shows drug binding sites of BSA.

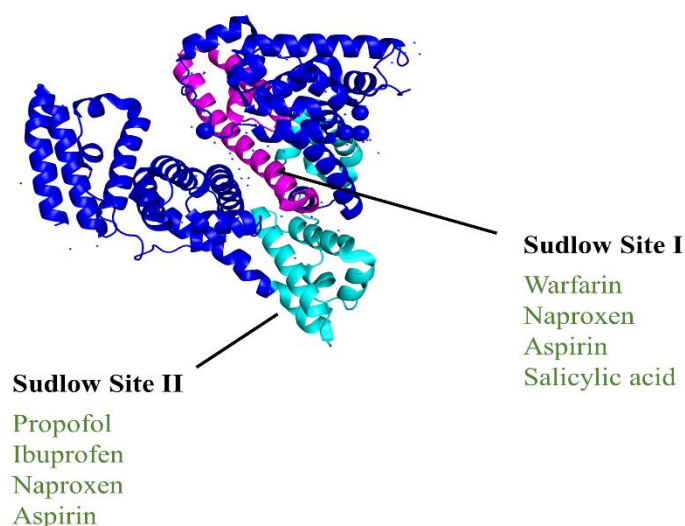


Figure 2.2 Three-dimensional structure of BSA and its drug-binding sites (the protein topology from PDB ID 4f5s).

Albumin has  $7 \pm 1$  high affinity binding sites for long chain fatty acids (FA). These binding sites are distributed throughout this protein. The first binding site is located in subdomain IB, which is also a site for binding polycyclic aromatic hydrocarbon epoxides. Site 2 is identified at the interface between IA and IIA, the third and fourth sites are located within subdomain IIIA, site 5 at subdomain IIIB, site 6 lies at interface between IIA and IIB, and site 7 is located in subdomain IIA [30]. The presence of amino acid residues in the first five fatty acid binding sites facilitates electrostatic/polar interactions with the carboxylic acid group of fatty acids [24]. It is important to note that the binding characteristics of BSA show high resemblance to that of HSA [25].

The secondary structure of BSA is composed of 67% helix, 10% turn, and 23% extended chain, and contains no  $\beta$ -sheet structure. pH, temperature, and various kinds of denaturants can modify the secondary as well as tertiary structures of albumin [31]. BSA contains 17 intrachain disulfide bridges and a free cysteine residue at position 34 (Cys34). The high stability of albumin arises from these disulfide bonds, which give some rigidity to each subdomain, while significant changes in the size and shape of the protein is possible under various external conditions [32]. Moreover, drugs can attach covalently to Cys34, which is located on the outer surface of albumin away from the main interior drug binding sites and has, therefore, been a focus for covalent conjugation of drugs [28].

Albumin hydrogels have in recent years gained increased attention. It is vital to choose the optimum method for preparing robust and biocompatible albumin hydrogels while maintaining the various functions of this protein such as ability to bind and release a wide range of molecules [27]. Therefore, if albumin hydrogel is used as a carrier, it is expected that a drug with high affinity to albumin is preferably loaded on the hydrogel and can be released slowly, as compared with hydrogels with no albumin [33].

In this thesis, three methods of hydrogel formation from BSA have been employed. In the first and second presented publications, BSA hydrogels are prepared by thermally and pH induced methods.

Numerous studies have been carried out to investigate heat-induced denaturation of BSA. In general, denaturation of BSA does not occur up to 40 °C. In the temperature range of 42 to 50 °C, BSA molecule undergoes reversible conformational changes, however, in the temperature range of 52 to 60 °C, the  $\alpha$ -helices content of BSA are irreversibly unfolded. From 60 °C, unfolding of BSA continues and  $\beta$ -aggregations of BSA are formed. At temperatures above 70 °C, the gelation by unfolding of BSA progresses further [31].

Thermally induced gelation requires two-stage sequential process. The first phase involves conformational changes in the protein with unfolding of some polypeptide segments, followed by a subsequent phase of protein-protein interaction leading to a formation of a network structure. In this state, protein gel consists of intermolecular cage-like structures, with the solvent continuous throughout the matrix. The physical and chemical properties of the protein influence the balance between attractive and repulsive forces which affect the matrix formation. During the first stage, the native state transits to the progel state, which results in protein denaturation. Meanwhile, intermolecular interactions is possible due to the availability of functional groups which were engaged in intramolecular hydrogen bonding and electrostatic interaction in the native state. Exposure of Hydrophobic groups leads to a hydrophobic interactions which are significant for gel network formation [34].

Albumin can undergo reversible conformational changes when exposed to different pH. For instance, by changing the pH from 7.4 to 3.5, albumin changes structure from N to F isoform. The former is the normal heart shape structure of albumin and the latter is the expanded cigar like shape. Reducing the pH to 2.7

enables albumin transition to the E isoform. In the pH-induced method, decreasing the pH from 7.4 to 3.5, changes the net charge on the protein from -16 mV to +100mV. In this condition, denaturation temperature of BSA changes from 62 °C to 46.8 °C. It has been observed that concentrated solution of BSA in the cigar like form (F isoform) can turn into a hydrogel network within 24 hours at room temperature (25 °C) or at 37 °C and in only 30 minutes. However, BSA protein in N isoform shows no gelation behavior unless the temperature increases above 62 °C, which triggers thermal denaturation of BSA [35-37].

In the first and second presented projects, BSA precursor solution was heated at 65 °C and 59 °C, which are above and below protein's denaturation temperature, to obtain thermally induced hydrogels. In order to obtain pH induced gels, hydrochloric acid (HCl 2 M) is added to the precursor solution of BSA and the pH is reduced to 3.5. By this method, it is possible to prepare hydrogels at 37 °C [38].

In the third presented publication, BSA hydrogels are prepared by addition of different amounts of ethanol into BSA precursor solution. The presence of alcohols as co-solvents of proteins above a certain concentration can alter the secondary structure of the proteins which results in their denaturation. The possible mechanisms for such effect can be explained as follows: the addition of alcohol can change the dielectric constant of the solvent, which modifies the electrostatic interactions among charged groups as well as hydrophobic interactions. Moreover, when alcohol is added to the protein aqueous solution, alcohol molecules can penetrate to protein core and form intramolecular hydrogen bonding, which promote  $\alpha$ -helical chain segment formation. However, intermolecular  $\beta$ -sheets can be formed due to metastability of  $\alpha$ -helical conformations. The common characteristics of both alcohol and thermally induced methods are the formation and increase of the intermolecular  $\beta$ -sheet structures upon aggregation and gelation process. It is important to mention that the nonpolar groups of protein molecules are kept protected from surrounding water by the hydrophobic effect, and when alcohols, which are not as polar as water, are presented as co-solvents, this hydrophobic effect is not so strong anymore which leads to the partial unfolding of proteins [39-41].

The effect of alcohols on secondary structure and conformational changes of proteins highly depends on the type of alcohol and its concentration. It has been

reported that low ethanol concentrations in the range of 0-20% does not significantly affect the secondary structure of the protein, while by increasing the concentration to 20-50%, the formation of  $\alpha$ -helical structures is promoted. However, at higher ethanol concentrations (above 50%),  $\beta$ -sheet structures are dominated and formed which induce aggregation and gelation [40].

The main investigation method used in this thesis is continuous wave electron paramagnetic resonance (CW EPR) spectroscopy. Electron paramagnetic resonance (EPR) spectroscopy is a highly sensitive and selective technique which can be used to detect paramagnetic centers or free radicals and provides profound insight in various fields of chemistry, materials science, and biomedical sciences [42, 43]. Most of the drug delivery systems cannot be studied by EPR spectroscopy due to lack of paramagnetic molecules or unpaired electrons. Therefore, by strategies like spin labeling or spin probing, which are based on covalent or non-covalent attachment of persistent reporter radicals such as organic nitroxide radicals into the drug, the protein, or both, it is possible to investigate the drug-protein interaction [20, 27].

Nitroxide compounds are persistent radicals with different physicochemical properties used frequently as model drugs or attached covalently to an active agent [44, 45]. Unique information such as microviscosity, and local polarities or pH can be obtained by analyzing the EPR spectra of nitroxides due to their sensitivity to the environment and changes in rotational motions, e.g. upon binding to a protein [46]. In all three publications presented in this work, diverse release mechanisms were studied through EPR spectroscopy, since various release patterns lead to different changes in the shape of the spectra [47]. EPR spectra are recorded usually in the form of first derivative. Therefore, by calculating the double integral of an EPR spectrum, it is possible to gain information on the signal intensity, which is directly proportional to the number of spins available in the system. In all of the projects, CW EPR was used to study the release behavior by plotting the double integral of the released spin-labeled drugs in the EPR spectra versus release time intervals, which is a measure of the released molecules. Another application of EPR is to study the interaction of spin labeled amphiphilic molecules such as fatty acids (FAs) with proteins like serum albumin. By this method, motional parameters as well as dynamic information like binding capacity of the protein can be obtained [48]. For instance,

immobilized radicals indicate slow rotational dynamics, while freely tumbling spin probes show no or little attachment to protein.

In the first publication, 16-doxy stearic acid (16-DSA), a spin-labeled stearic acid at position 16 from the carboxylic acid head group, is used as a model tracer molecule for amphiphilic drugs and the release behavior and interaction of this FA with BSA is investigated in detail.

In the second publication, spin-labeled coumarin-3-carboxylic acid (SL-CCS) and warfarin (SL-WFR) are selected as SL-pharmaceutical and effect of different parameters such as type of drug, drug concentration, duration of gel formation and gelation method on release rate and behavior of these two SL-drugs are thoroughly studied.

Coumarin and warfarin are the most widely prescribed anticoagulant drugs for the treatment of cardiovascular diseases, which are the main cause of mortality worldwide. Myocardial infarction or strokes are the reasons of cardiovascular death, which are mostly due to an atherosclerotic process. Atherosclerosis is a serious condition where inappropriate clots are formed within intact arteries [49]. Most of the anticoagulants suffer from limited therapeutic efficacy due to their hydrophobic nature. Coumarinic derivatives are natural or synthetic anticoagulant drugs and are popular due to their importance in medicine. However, they have shown narrow therapeutic window and high variability in dose-response. Warfarin and coumarin, which are coumarinic derivatives, are oral anticoagulants for thromboembolic disorders treatment. Controlled delivery of such drugs can avoid problems such as high fluctuation in dose-response, narrow therapeutic range and considerable interactions with other medications [7, 20, 49, 50].

In the third publication, release behavior of SL-naproxen (SL-NPX) from BSA hydrogels prepared by ethanol induced method is studied.

Non-steroidal anti-inflammatory drugs (NSAIDs) are widely used in the treatment of rheumatoid arthritis, osteoarthritis, inflammation, acute gout, metastatic bone pain, headaches and migraines. Naproxen is a potent NSAID, which relieves fever, inflammation and pain in joints and muscles. Due to short bioavailability of the drug (8 hours) by oral administration, repeated dosing is required to maintain pharmacological level. However, frequent administration in patients with chronic inflammatory diseases who require long treatment with naproxen can lead to



gastrointestinal disorder and bleeding. Therefore, it seems crucial to develop a controlled drug delivery system to reduce the frequency of administration and allow the sustained release of drug [5, 51, 52]. Figure 2.3 shows the chemical structures of 16-DSA and all SL-pharmaceuticals used in this thesis.

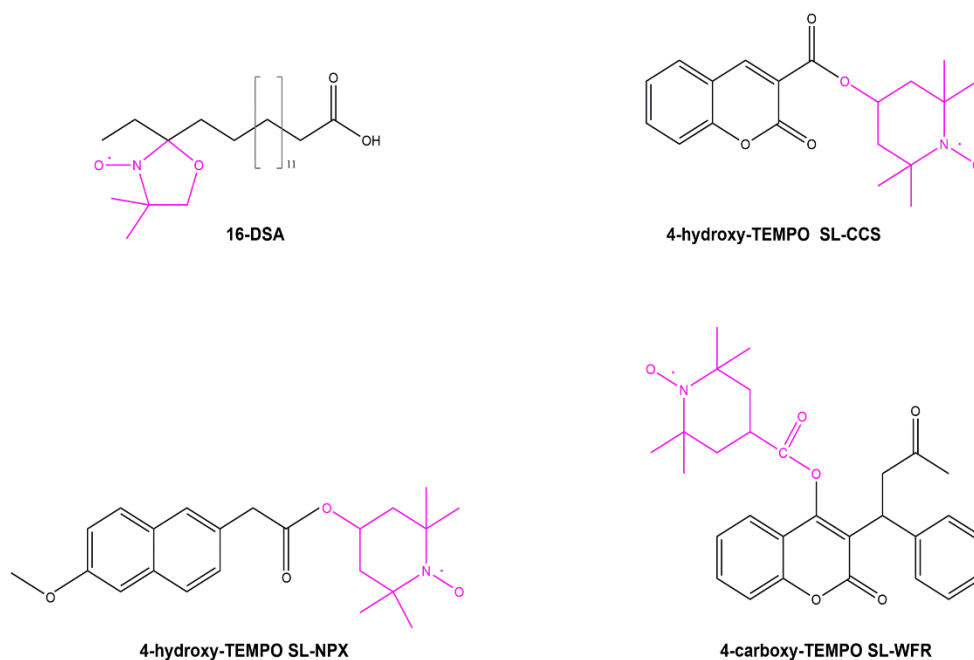


Figure 2.3 Chemical structure of 16-DSA and SL-pharmaceuticals studied in this thesis.

The aim of this dissertation is directed towards the development of controlled drug delivery systems based on BSA hydrogels that are prepared by different methods, namely thermally, pH and ethanol induced techniques, and study the release behavior of 16-DSA as an amphiphilic model drug, and different SL-pharmaceuticals such as SL-CCS, SL-WFR, and SL-NPX. The objective of the present contribution is to investigate the effect of different parameters such as method of gel formation, drug concentration, and the incubation time, which is the time required for gelation to process at specific temperature or pH, on release rate. The investigation is completed by studying the influence of such parameters on the mechanical properties of the hydrogels by rheology, the secondary structure of the protein during gelation using ATR-IR spectroscopy, the interaction of SL-drugs with BSA by means of CW EPR spectroscopy, and the size and nature of released components by DLS.

This cumulative dissertation consists of three publications. A list of publications

is presented prior to introduction. The second chapter is the general introduction to the content of this thesis, which is followed by a theoretical chapter that briefly explains different characterization methods used in the publications. An overview over the published papers and reprints of the three published papers are assembled in chapter four. In the fifth chapter, the results of the papers are discussed in detail and the sixth chapter reaches conclusions and presents an outlook in the research field.

### **3 Theory and Methods**

The following chapter presents a brief introduction on the most important methods used throughout the thesis. Rheological characterization is used to obtain information about the mechanical properties and viscoelastic behavior of different hydrogels prepared by different methods. Changes in the secondary structure of the protein during gelation is investigated by ATR-IR spectroscopy. CW EPR spectroscopy is used to study the interaction of SL-drug-BSA and release behavior. Moreover, in the second paper, the percentage of drug inside the hydrogel as well as spatial distribution of SL-pharmaceuticals is investigated by means of electron paramagnetic resonance imaging (EPRI). The insight about the size and nature of released components is gained via DLS.

#### **3.1 Rheology**

The essential parameters in the design of hydrogels for pharmaceutical and biomedical applications are mechanical and viscoelastic properties. The rigidity and integrity of gels gain importance in the field of drug delivery, since the hydrogel acts as a carrier and protects the therapeutic agent, until the agent is released from the system. On the other hand, the flowability of gel plays a significant role when it is used as an injectable carriers for drug delivery applications [20, 27].

The majority of materials show a mixture of viscous and elastic behavior when sheared, called viscoelastic behavior. To understand the definition of the rheological parameters which are required for description of deformation behavior, the two-plate model is used [53].

The viscoelastic behavior is measured by performing oscillatory test between the two plates of the rheometer (Figure 3.1) [53].

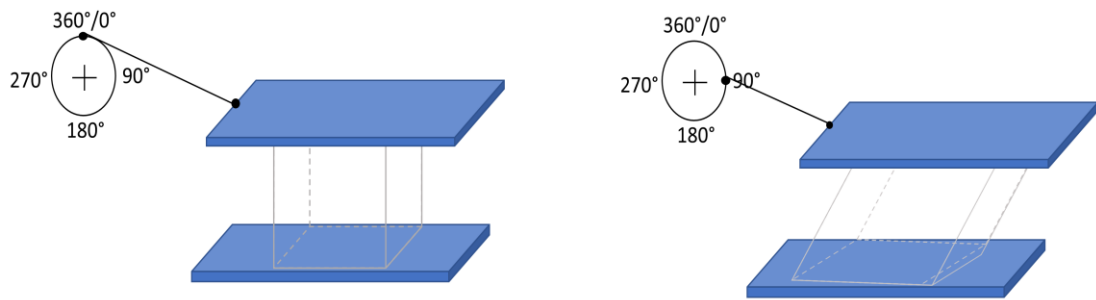


Figure 3.1 The two-plate model with driving wheel and push rod for shear tests used for oscillatory test. The deflection of the upper plate at different angle positions  $0^\circ / 90^\circ / 180^\circ / 270^\circ / 360^\circ$  of the rotating wheel is illustrated [53].

A shear stress ( $\tau = \frac{F}{A}$ , with shear stress  $\tau$ , shear force  $F$  (in N) and shear area  $A$  (in  $\text{m}^2$ )) is applied to the sample, which is placed on the stationary rheometer's plate, while the upper plate moves back and forth parallel to the lower plate by a driving wheel. The oscillating frequency is constant, since a constant rotational speed is applied. Strain or deformation ( $\gamma = \frac{s}{h}$ , with shear strain  $\gamma$ , deflection path  $s$  (in m), and shear gap  $h$  (in m)) can be calculated by measuring the deflection path of upper plate. By plotting strain against time, while the driving wheel is rotating, a sine curve with the strain amplitude ( $\gamma_A$ ) is obtained (Figure 3.2) [53].

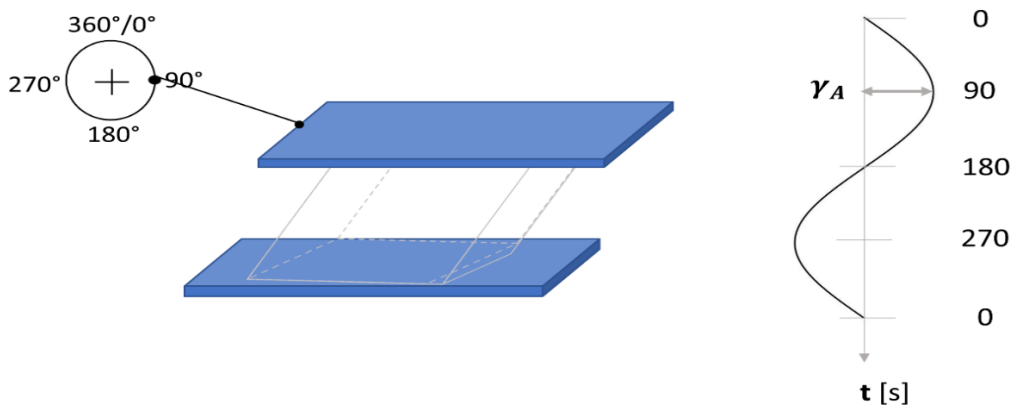


Figure 3.2 The two-plate model used for oscillatory test shown on the left. Time-dependent strain value with the amplitude  $\gamma_A$  of the upper plate is shown on the right. A full turn of the driving wheel results in a complete sine curve [53].

Parameters for oscillatory tests are usually preset in the form of a sine curve. For the two-plate model the test is a controlled sinusoidal strain test. The

amplitude (maximum deflection) and the oscillation period (blue line in Figure 3.3) describe the sine curve. The oscillation frequency is the reciprocal of the oscillation period (Figure 3.3) [53].

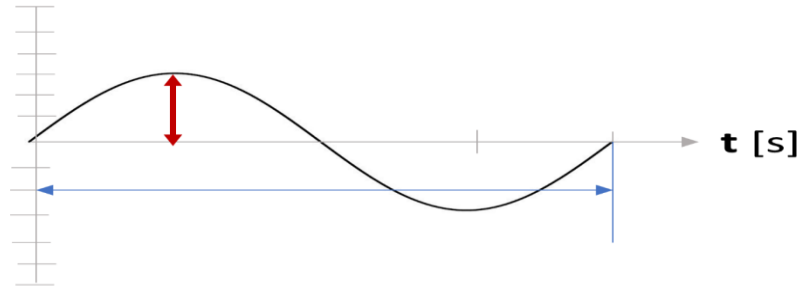


Figure 3.3 A sine curve is determined by its amplitude (maximum deflection) and its oscillation period or frequency [53].

Shear stress ( $\tau$ ) is a counter force which keeps the lower plate in position and when the sample does not have a large deformation, sinusoidal curve of the shear stress with the amplitude ( $\tau_A$ ) can be obtained by plotting shear stress over time. Both preset and response curves have the same oscillatory frequency. For rigid materials with elastic behavior such as steel or stone, there is no time lag between the preset and the response sine curve. However, most of the samples show viscoelastic behavior, therefore there is a time lag between these sine curves which is called phase shift ( $\delta$ ) and is always between  $0^\circ$  and  $90^\circ$  [53-56]. To describe the viscoelastic behavior of the hydrogels, storage and loss moduli are measured. In general, storage modulus ( $G'$ ) characterizes the elastic characteristics (stored energy) and loss modulus ( $G''$ ) represents the viscous portion (dissipated energy). Equations 3.1 and 3.2 define the two moduli. The values of  $G'$  and  $G''$  are important for gelation process. In the liquid or sol state,  $G'' > G'$ , at the gelation point,  $G'' = G'$ , and in the gel state,  $G' > G''$  [54].

$$\text{Storage modulus:} \quad G' = \frac{\tau_A}{\gamma_A} \cos\delta \quad (3.1)$$

$$\text{Loss modulus:} \quad G'' = \frac{\tau_A}{\gamma_A} \sin\delta \quad (3.2)$$

$\tau/\text{Pa}$  = shear stress

$\gamma/\%$  = deformation

$\delta/^\circ$  = phase shift angle

### 3.2 ATR-IR spectroscopy

Attenuated Total Reflection (ATR) Fourier Transform Infrared Spectroscopy (FTIR) techniques are widely used to characterize the protein secondary structure content [57]. The two major vibrational bands of proteins are amide I and amide II. The former is the most sensitive band, corresponding to the stretching vibration of C=O bonds, which is found between 1600 and 1700  $\text{cm}^{-1}$ . The latter is originating from the bending vibration of N-H bonds which occurs at 1500-1600  $\text{cm}^{-1}$  [58].

In the first publication, ATR-IR spectroscopy is used to study changes in the secondary structure of BSA during gelation alone, and in the presence of fatty acids. In the third publication presented in this thesis, this method is performed to investigate how different ethanol concentrations cause changes in the secondary structure of BSA during hydrogel formation.

ATR is based on internal reflectance. An infrared (IR) beam travels from a crystal with high refractive index ( $n_c$ ) to a sample with lower refractive index ( $n_s$ ). The incoming beam makes an angle with the surface which is denoted as angle of incidence,  $\theta_i$ . If the angle of incidence is small, some amount of the light is reflected back into the crystal, and some of the beam will refract out into the low refractive index medium. At a particular angle of incidence, the angle of refraction ( $\theta_R$ ) will become  $90^\circ$ , and almost all of the light waves are reflected back, the phenomena called *total internal reflectance*. Total internal reflection will take place at critical angle ( $\theta_c$ ), which is the minimum angle at which total internal reflectance occurs in a material, and all angles greater than  $\theta_c$ . Critical angle is a function of the refractive indices of both the sample and crystal as follows [59, 60]:

$$\theta_c = \sin^{-1} n_s/n_c \quad (3.3)$$

Since the sine of angle cannot be greater than 1, total internal reflectance ceases when  $n_s$  is greater than  $n_c$ . Since the IR beam does not leave the crystal, at the point of internal reflectance the incoming and outgoing beams undergo constructive interference. Therefore, at this point the amplitude of IR will be greater than the amplitude on each side. The IR light reaches above the surface of the crystal into the medium with lower refractive index by less than a micron to

10 microns, which is called evanescent wave [59, 60].

The intensity of the evanescent wave decreases exponentially with distance above the surface of the ATR crystal. When the sample is applied on the crystal and it is in contact with evanescent wave, the sample absorbs some of the beam's energy. Hence, the intensity of the reflected infrared beam reduces at this point, and therefore the term attenuated total reflectance (ATR) is used. This absorbance is translated into the IR spectrum of the sample [59-61].

### **3.3 Continuous Wave Electron Paramagnetic Resonance (CW EPR) Spectroscopy**

In all three publications, CW EPR spectroscopy is used to provide information on the released components and the interaction of SL-drugs and fatty acid with albumin-derived materials, and their bound states. Moreover, release mechanisms are determined by plotting the double integral values of first derivative EPR spectra versus release time. The principles and applications of EPR spectroscopy are described in great detail in various publications and books, therefore, a short introduction on the basics of this method is given in this thesis.

Electron paramagnetic resonance, also known as electron spin resonance, is a powerful and noninvasive spectroscopic tool, which can be used to detect and characterize paramagnetic species with one or more unpaired electrons in their orbitals. EPR shows greater sensitivity than nuclear magnetic resonance (NMR), since its resonance frequency is  $10^3$  higher due to larger magnetic moment of an electron, therefore, it is possible to detect free radical concentrations as low as 0.5-1 nmol/ml by this method [47].

The majority of materials, except for paramagnetic transition metal ions that possess intrinsic free radicals, are not detectable by EPR due to the absence of paramagnetic centers. It is well known that covalent chemical bonds are based on pairing of electrons, and hence due to their diamagnetic properties, EPR spectroscopy can investigate only few macromolecular systems. To achieve more information on different systems, spin labeling or spin probing techniques can be used by covalent or non-covalent incorporation of paramagnetic substances such as organic nitroxide radicals, conventionally presented with the structural unit RNO, into the drug, the protein, or both. Therefore, it is possible to

study drug–protein interactions in drug delivery systems. Furthermore, through this method, information about the local environment, motional parameters, and ligand binding of the protein can be obtained [27, 42, 62].

The intrinsic property of electrons, the negatively charged particles, is spin, characterized by the spin angular momentum  $\mathbf{S}$ . The spin angular momentum can be defined with the magnetic quantum number  $m_s = \pm 1/2$ , resulting in two individual spin states, denoted as ‘spin-up’ ( $m_s = +1/2$ , called the  $\alpha$ -spin) and ‘spin-down’ ( $m_s = -1/2$ , called the  $\beta$ -spin). In the absence of a magnetic field, the energy of the two electron spin levels are the same and the probability of the electron being in either spin state is equal. In order to split the energy levels of the initial degenerated spin states, the electron needs to be subjected to an external magnetic field ( $B_0$ ). The interaction energy ( $E$ ) of an electron with  $B_0$  is given by:

$$E = g_e \mu_B m_s \times B_0 \quad (3.4)$$

$g$  =  $g$ -factor ( $g = 2.0023$  for free radicals)

$\mu_B$  = Bohr magneton

$B_0$  = strength of the applied magnetic field

When the spin of an electron is placed in an external magnetic field, the electron spin has only two possible orientations relative to the magnetic field. The electron spin will either occupy the lower energy state when they align parallel to the direction of applied magnetic field or higher energy state in which the spin is aligned against the external magnetic field. The splitting of the electron spin energy in a magnetic field referred to as the *electron Zeeman levels*. In EPR spectroscopy, a sample containing unpaired electrons irradiated with electromagnetic radiation ( $h\nu$ ) in the presence of an external magnetic field. The resonance condition is satisfied between the lower and upper energy states when electromagnetic radiation corresponding to  $\Delta E$  is applied to the sample (Figure 3.4) [62, 63].



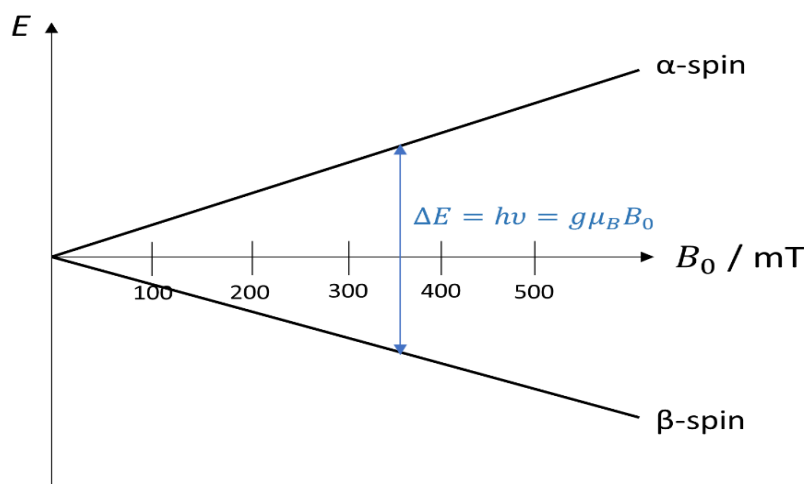


Figure 3.4 The electron Zeeman levels for an unpaired electron subjected to an external magnetic field ( $B_0$ ) [63].

The energy difference between these two states is determined by the equation given below:

$$\Delta E = h\nu = g_e\mu_B B_0 \quad (3.5)$$

$h$  = Planck's constant

$\nu$  = frequency of electromagnetic radiation

The interaction of the unpaired electron with an applied magnetic field is not the only effect detectable by EPR spectroscopy. The nuclei have also a magnetic spin, resulting in further magnetic interactions in the electron spin system, which leads to multi-line EPR spectrum that contains a wealth of information. A nuclear Zeeman splitting is the result of the interaction of the nuclear spin with the applied external magnetic field. The interaction of unpaired electron with magnetic nuclei produces splitting in the energy levels of EPR spectrum, which is called hyperfine splitting. These interactions create small but considerable perturbations to the electron spin energies ( $E$ ), which are summarized as:

$$E = g\mu_B B m_s - g_N \mu_N B m_l + a m_s m_l \quad (3.6)$$

$g_N$  = nuclear  $g$ -factor (which can have positive or negative values)

$\mu_N$  = nuclear magneton

$a$  = hyperfine splitting constant

Protons, like electrons can possess an orbital and spin angular momentum. Nuclei that have a non-zero nuclear spin quantum number,  $I$ , will possess an associated magnetic moment  $\mu_I$  as well. In analogy with the electron magnetic moment, the influence of a magnetic field can remove the degeneracy of the nuclear energy levels. Therefore, the magnetic dipole moments of the nuclei will align parallel or antiparallel to the direction of applied magnetic field. Comparing to the electron Zeeman levels, the nuclear Zeeman energy levels are equally spaced and are considerably smaller than the electron Zeeman splitting due to much smaller  $\mu_N$  value [63].

Figure 3.5 shows energy level diagram for a spin system with  $S = I = 1/2$ . Each of the non-degenerate electron Zeeman levels is split into two nuclear Zeeman levels. This leads to four discrete energy levels ( $E_1$  to  $E_4$ ) for an  $I = 1/2$  system, because of the combined interaction of the electron and nuclear magnetic dipole moments with the applied external magnetic field [63, 64].

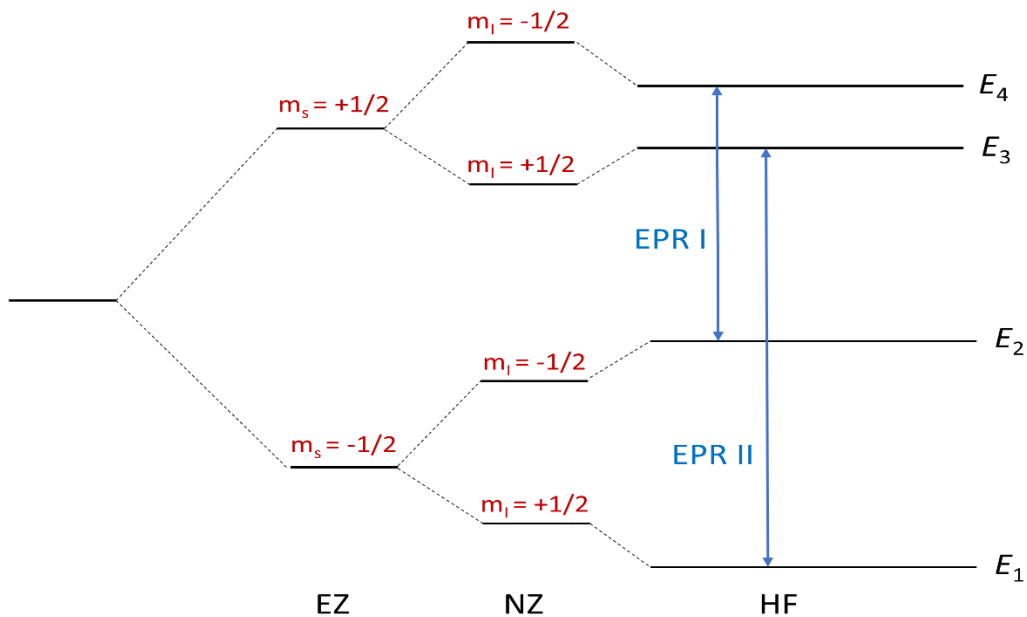


Figure 3.5 Energy diagram in a fixed magnetic field for a spin system with  $S = I = 1/2$ , showing the electron Zeeman (EZ), nuclear Zeeman (NZ) and hyperfine interaction (HF). The two allowed EPR transitions lead to the experimentally observed resonances labelled EPR I and EPR II [63].

As it was explained above,  $am_s m_I$  in equation 3.6, describes the hyperfine interaction arising from the interaction between the electron and nuclear magnetic dipole moments. The hyperfine interaction can create a perturbation of the nuclear Zeeman energy levels towards higher or lower energy. The

magnitude of the interaction determines the extent of this perturbation which is described by the hyperfine splitting  $\alpha$  [63].

The solutions to equation 3.6 for the corresponding energies of the system with  $m_s = \pm 1/2$  and  $m_I = \pm 1/2$  are given by:

$$E_1 = -\frac{1}{2}g_e\mu_B \cdot B - \frac{1}{2}g_N\mu_N \cdot B - \frac{1}{4}a \quad (3.7a)$$

$$E_2 = -\frac{1}{2}g_e\mu_B \cdot B + \frac{1}{2}g_N\mu_N \cdot B + \frac{1}{4}a \quad (3.7b)$$

$$E_3 = +\frac{1}{2}g_e\mu_B \cdot B - \frac{1}{2}g_N\mu_N \cdot B + \frac{1}{4}a \quad (3.7c)$$

$$E_4 = +\frac{1}{2}g_e\mu_B \cdot B + \frac{1}{2}g_N\mu_N \cdot B - \frac{1}{4}a \quad (3.7d)$$

The energy diagram shown above in Figure 3.5 arises from positive  $g_N$  and  $\alpha$ . In CW EPR spectroscopy, the highest probability for transitions from one state to another occurs when  $\Delta m_s = \pm 1$  and  $\Delta m_I = 0$ . In other words, the electron spin state must change as a result of the transition, while the nuclear spin state must remain the same. Therefore, for the system with two spins shown in Figure 3.5, two EPR transitions are allowed to take place which are labelled EPR I ( $E_2 \rightarrow E_4$ ) and EPR II ( $E_1 \rightarrow E_3$ ). As can be seen in this figure, these two transitions have different arrow lengths, representing different energy quanta needed to induce transitions, leading to two resonance lines in EPR spectrum. The hyperfine splitting constant is defined by the magnitude of the separation between these two resonance lines:

$$| E_1 \rightarrow E_3 | - | E_2 \rightarrow E_4 | = \alpha \quad (3.8)$$

Hyperfine splitting constant can be obtained by calculating the distance between the first and second peaks in EPR spectrum [63].

The number of lines and their intensities in an EPR spectrum can be determined by the type and number of nuclei interacting with the electron. In general, there are  $2I+1$  energy levels for each  $m_s$  value, considering an unpaired electron which experiences a hyperfine interaction with a nucleus of spin  $I$ . Therefore, there are  $2I+1$  EPR transitions between these levels, and consequently, the EPR spectrum of a radical experiencing a hyperfine interaction with a nucleus of spin  $I$

demonstrates  $2I+1$  lines [63].

The spin labels used in this thesis have a nucleus  $^{14}\text{N}$  with nuclear spin of  $I = 1$ , resulting in triplet splitting in an external magnetic field. Therefore, the interaction of the electron spin states with the three nuclear spin states yields three possible allowed transitions and hence gives three signals in an EPR spectroscopy experiment (see Figure 3.6). In contrast, only two lines can be seen in the EPR spectrum of the  $^{15}\text{N}$  spin probes due to the interaction of the unpaired electron with the nuclear spin of the  $^{15}\text{N}$  nuclei ( $I = 1/2$ ) [63].

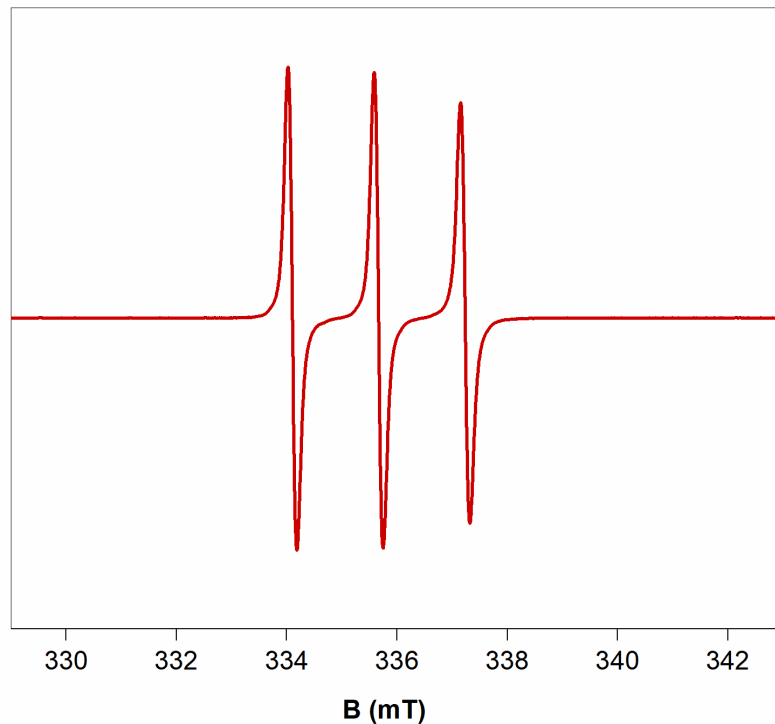


Figure 3.6 Typical nitroxide triplet EPR signal.

It is possible to gain information about the rotational diffusion of a spin probe or a spin label molecule by determining the rotational correlation time  $\tau_c$ , which can be roughly categorized into isotropic limit ( $\tau_c \leq 1$  ps), fast motion ( $\tau_c \approx 0.1$  ns), slow motion ( $\tau_c \approx 1$  ns), and rigid limit ( $\tau_c \geq 1$   $\mu\text{s}$ ). Rotational correlation time  $\tau_c$  can be gained from rigorous simulation of EPR spectra, which is calculated from diffusion tensor  $D$ :

$$\tau_c = \frac{1}{6} (D_{xx}D_{yy}D_{zz})^{-\frac{1}{3}} \quad (3.9)$$

The tumbling behavior of the nitroxyl radicals can be influenced by the

microviscosity of the environment. Low viscous media result in free tumbling leading to highly symmetric spectra with three narrow lines and rotational correlation time  $\tau_c$  in the range of 0.01-0.1 ns. By contrast, the molecular tumbling rate of nitroxyl radical decreases in high viscous media. Because of the restricted motion, the anisotropy of hyperfine interaction is only partially or not averaged, leading to a line broadening, a decrease in a signal intensity and an increase in  $\tau_c$  [47].

In addition to information about the dynamics, EPR spectroscopy provides insight about the local environment of the spin probes as well. The electronic structure of a nitroxide slightly changes, depending on the interactions between molecules and their surroundings, which can influence the hyperfine splitting initiated by  $^{14}\text{N}$ . Therefore, the same kind of spin probe can show deviations in the isotropic hyperfine coupling constant  $a_{\text{iso}}$  in solvents with different polarities. High polar environments result in larger  $a_{\text{iso}}$  values, while smaller hyperfine couplings are indicative of lower polarities [38].

Normally, EPR spectra are displayed as first derivative spectra. In other words, the slope of the absorption spectrum is plotted as a function of magnetic field strength, as opposed to the absorption spectrum itself [27].

In EPR, the microwave frequencies used for measurement are classified into bands (see Table 3.1). Within each band, a range of frequencies is possible. However, the ones denoted in Table 3.1 show the most common frequencies. The units of field are given in Tesla (T) for  $g = 2.0023$ . Therefore, the exact values for the magnetic field at which transitions occur depend on the chosen band.

Commonly used EPR frequency bands in drug delivery researches are X-band and L-band, which correspond to the microwave ranges of 10 GHz and 1 GHz, respectively. The X-band spectrometer has lower microwave penetration depth (0.5-1 mm) in water-containing samples due to high dielectric constant that results in microwave absorption of water or other liquids with high polarities. Although, it is possible to measure suspensions, emulsions and isolated skin by X-band by means of capillaries or tissue cells [38, 41, 47, 63, 65].

Table 3.1 Common microwave frequency bands used in EPR spectroscopy [66].

<b>Band</b>	<b>Frequency [GHz]</b>	<b>Magnetic Field [T]</b>
L	1	0.036
S	3.5	0.13
X	9.5	0.34
Q	34	1.21
W	95	3.4

### 3.4 Dynamic Light Scattering (DLS)

To gain deep insight on the size and nature of the released components, DLS is used in all three publications presented in this thesis. The intensity-time correlation function for different release time is studied and compared in detail.

In general, DLS is a nondestructive technique for characterization of complex liquids, proteins, polymers and colloidal structures. By this method, it is possible to determine size, size distributions and in some cases the shape of nanoparticles. When a solution containing macromolecules is irradiated by a monochromatic beam, the macromolecules scatter the light in all directions according to their size and shape. In dynamic light scattering, the diffusion coefficient ( $D_t$ ), which provides information on the hydrodynamic size of macromolecules in solution, can be obtained by analyzing the intensity fluctuations of scattered light. Furthermore, DLS measures Brownian motion of the macromolecules and relates this motion to the size of the particle. Brownian motion, which depends on the size, temperature and solvent viscosity, is the random movement of particles due to the bombardment by the solvent molecules. Size of macromolecules can be calculated by monitoring the movement of particles over a time range. Large particles move slower and therefore they adopt a specific position, while smaller particles diffuse faster, resulting in different positions at different time points [67-69].

The hydrodynamic radius, the radius of a hypothetical sphere that diffuses at the same rate as particle under investigation, is calculated from the translational

diffusion coefficient by using the Stokes Einstein equation:

$$D_{\tau} = \frac{K_B T}{6\pi\eta R_h} \quad (3.10)$$

$D_{\tau}$  = translational diffusion coefficient

$K_B$  = Boltzmann coefficient

$T$  = absolute temperature

$\eta$  = viscosity of medium

$R_h$  = hydrodynamic radius

The translational diffusion coefficient depends on several parameters such as size of the particle core and its surface structure, as well as concentration and type of ions in the medium [70].

The particle diffusion speed can be affected by the total ion concentration of the medium by changing the thickness of the electric double layer called the Debye length. Therefore, a low conductive medium makes an extended double layer of ions around the particle, decreasing the diffusion speed and leading to a larger hydrodynamic diameter [70].

The size of the particle can be deeply affected by any change to the surface of a particle which influences the diffusion speed. The diffusion speed decreases more when an adsorbed polymer layer projects out into the medium, than if the polymer is lying flat on the surface [70].

All techniques describing the size of non-spherical particles have an inherent problem. The only object whose size can be determined by a single measure is the sphere. As mentioned before, the hydrodynamic diameter of a non-spherical particle is defined as the diameter of a sphere which has the same translational diffusion speed as the particle. The hydrodynamic size can be changed when the shape of a particle changes in a way that influences diffusion speed. For instance, even small changes in the length of a rod-shaped particle can impact the hydrodynamic size, while changes in the diameter of the rod is hard to detect since it barely affects the diffusion speed [67-71].

In a DLS instrument, a detector records the scattering intensity, since the incident light is scattered in all directions due to the irradiation of laser light into the particles in solution. The scattered light may have either constructive or

destructive phase. The former leads to a detectable signal production, while in the latter the scattered light cancel each other out (Figure 3.7). The detector position can be at  $90^\circ$  (side scatter),  $173^\circ$  (back scatter) and  $158^\circ$  (close to the incident light of  $180^\circ$ ) [70].

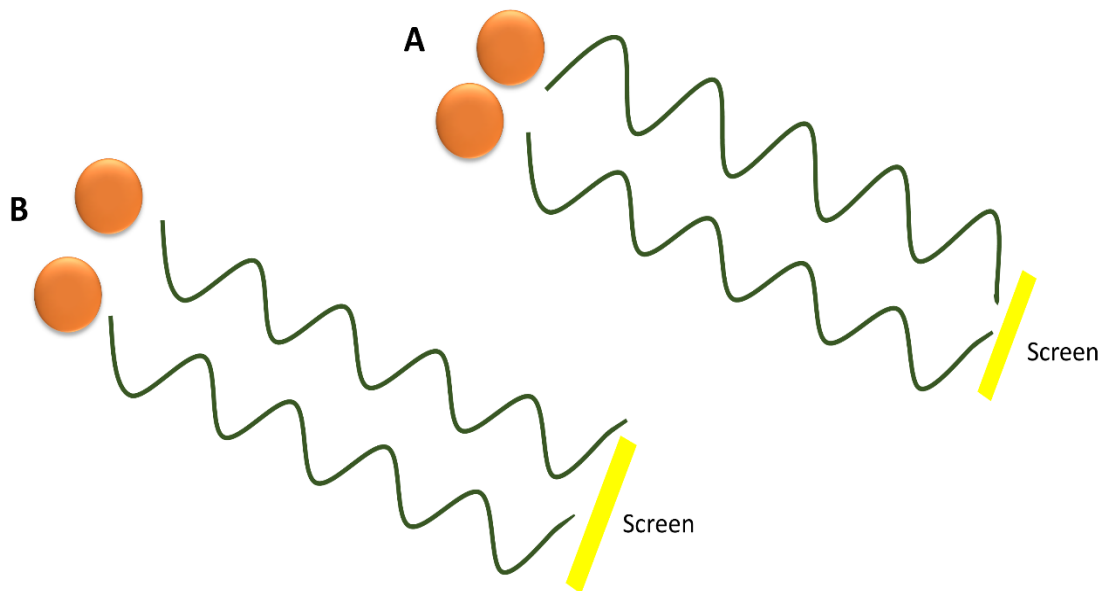


Figure 3.7 (A) shows two beams interfere and cancel each other out leading to a decreased intensity detected. (B) displays two beams interfere and enhance each other resulting in an increased intensity detected [70].

Typical intensity fluctuations as a result of a dispersion of small particles and a dispersion of large particles are schematically shown in Figure 3.8. The small particles lead to more rapid intensity fluctuation than the larger ones [70].

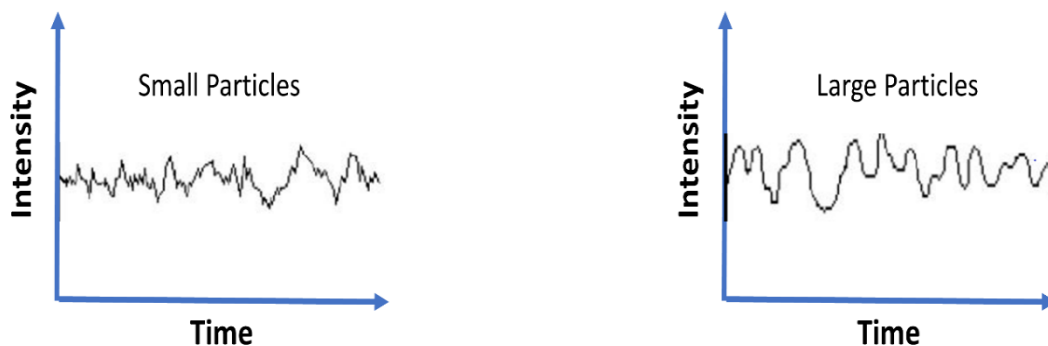


Figure 3.8 Typical intensity fluctuations of small and large particles [72].



## 4 Results

### 4.1 Overview over the publications

The published papers presented in this thesis aimed at investigating release behavior of a fatty acid (serving as an amphiphilic model drug) and different SL-pharmaceuticals from hydrogels made from BSA. For this purpose, the release profiles of a model drug and SL-drugs from BSA hydrogels prepared with different methods are compared in detail.

In this work various properties of these hydrogels are described at three levels: (i) their mechanical and viscoelastic (macroscopic) behavior (via rheological characterization), (ii) changes in the secondary structure of the protein (nanoscopic level) during gel formation through ATR-IR spectroscopy and (iii) the hydrogel-fatty acid/SL-drugs interaction using CW EPR spectroscopy.

All publications intended to elucidate the combined influences of fatty acid/ type of drug, their concentration, duration of gel formation and gelation methods on the release behavior.

#### 4.1.1 Nanoscopic characterization of stearic acid release from bovine serum albumin hydrogels

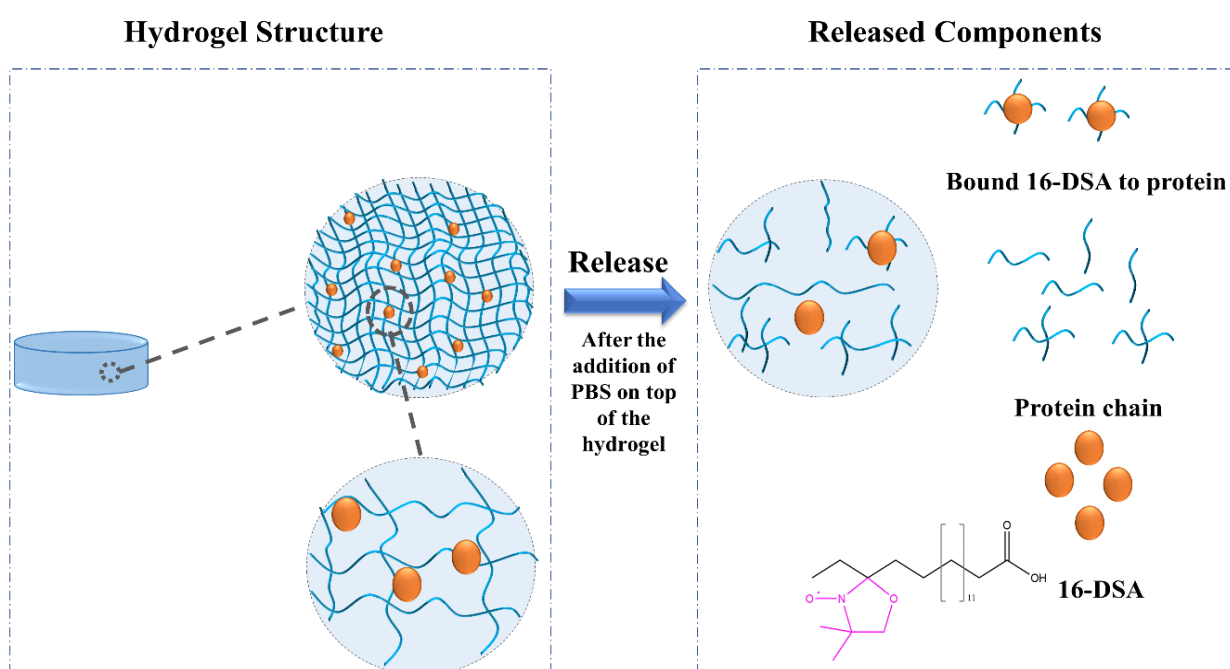


Figure 4.1 Schematic representation of 16-DSA release from hydrogels studied in this paper.

Serum albumin is the most abundant protein in the circulatory system of mammals, reaching a concentration of 40 to 50 mg ml<sup>-1</sup> in plasma, and it is a remarkably versatile carrier for drugs, fatty acids, hormones and polypeptides which can attach through physical or covalent bonding to the binding sites of this protein [31, 38]. Albumin is being considered in many biomaterials science studies and drug delivery applications due to its low toxicity and immunogenicity, high biocompatibility, biodegradability, high stability and availability at high purity and low cost [27, 73].

In this project, the release behavior of 16-DSA, which serves as a model tracer molecule for amphiphilic drugs, from BSA hydrogels was investigated.

In the first part of this paper, BSA hydrogels, prepared by two different procedures, namely thermally and pH induced methods were characterized. Mechanical and viscoelastic behavior of the hydrogels during gel formation in the presence and absence of fatty acid were studied using rheological characterization. Hydrogels obtained by thermally induced method at 65 °C and 59 °C, which are above and below denaturation temperature of BSA (62 °C), were mechanically tough hydrogels. Therefore, it is possible to prepare robust hydrogels even below denaturation temperature of BSA. To gain deep insight on the secondary structure changes of protein during gelation, ATR-IR measurements were performed, which showed the formation of  $\beta$ -sheet structure (by emergence of the two peaks at about 1620 and 1680 cm<sup>-1</sup>) and reduction of  $\alpha$ -helix content.

In the second chapter of this study, the effects of 16-DSA concentration, gel preparation method, hydrogel incubation time (the time at which gelation is processing at specific temperature or pH) on the release profile of 16-DSA were studied by CW EPR spectroscopy. Release rates were calculated by double integration of the first-derivative CW EPR spectra. Moreover, molecular insights were obtained from EPR spectral simulations, which gave information on the relative percentages of tightly and intermediately bound 16-DSA to BSA and freely rotating 16-DSA in both hydrogels and release medium. Furthermore, the size and nature of released components were investigated by analyzing the autocorrelation functions obtained from DLS measurements during release from hydrogels prepared by different methods.

#### 4.1.2 Molecular-level release of coumarin-3-carboxylic acid and warfarin-derivatives from BSA-based hydrogels

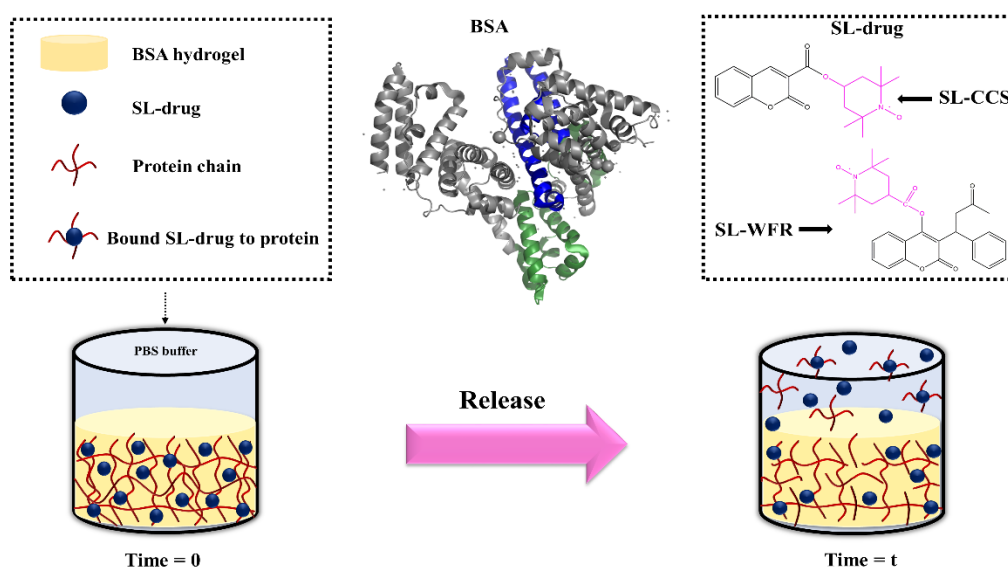


Figure 4.2 Schematic representation of SL-warfarin and SL-coumarin-3-carboxylic acid release from BSA hydrogels.

Thromboembolic disorders are among the most common and often fatal cardiovascular diseases. Two widely prescribed drugs for the treatment of such diseases are coumarin and warfarin. Oral administration of these types of drugs suffers from variability in dose response and narrow therapeutic window. Therefore, controlled delivery of such drugs can prevent problems related to high fluctuation in dose-response, narrow therapeutic range and considerable interactions with other medications [7, 20, 50].

The goal of this project was to develop and compare controlled delivery systems based on BSA hydrogels and SL-CCS and SL-WFR as candidate drugs to investigate their release behavior from the prepared gels.

The methods of gel formation, namely thermally and pH induced methods, used in this paper were the same as in the previous publication. The mechanical properties of hydrogels during gelation and the impact of CCS and WFR on gelation kinetics were studied in depth via rheological measurement. It seemed that the addition of both drugs weakened the mechanical properties.

We used CW EPR spectroscopy and EPRI to study the effects of drug concentration, the method of gel formation, and incubation time on release behavior of the mentioned SL-drugs. The combination of both techniques allows

better observation of release behavior, since the former was used to analyze the release medium, while the latter shed light on the spatial localization of a spin probe in a nondestructive way and followed the position of probes inside the slowly dissolving gels. Differences in chemical substitutions of SL-CCS and SL-WFR and binding capacities of BSA for SL-pharmaceuticals could affect drug-protein interactions as well as release rate. Moreover, drug loading could affect the release behavior, as lower drug to BSA molar ratios led to a second sustained release phase, while higher drug to BSA molar ratios showed zero-order release kinetics.

#### 4.1.3 Macro- and nanoscale effect of ethanol on bovine serum albumin gelation and naproxen release

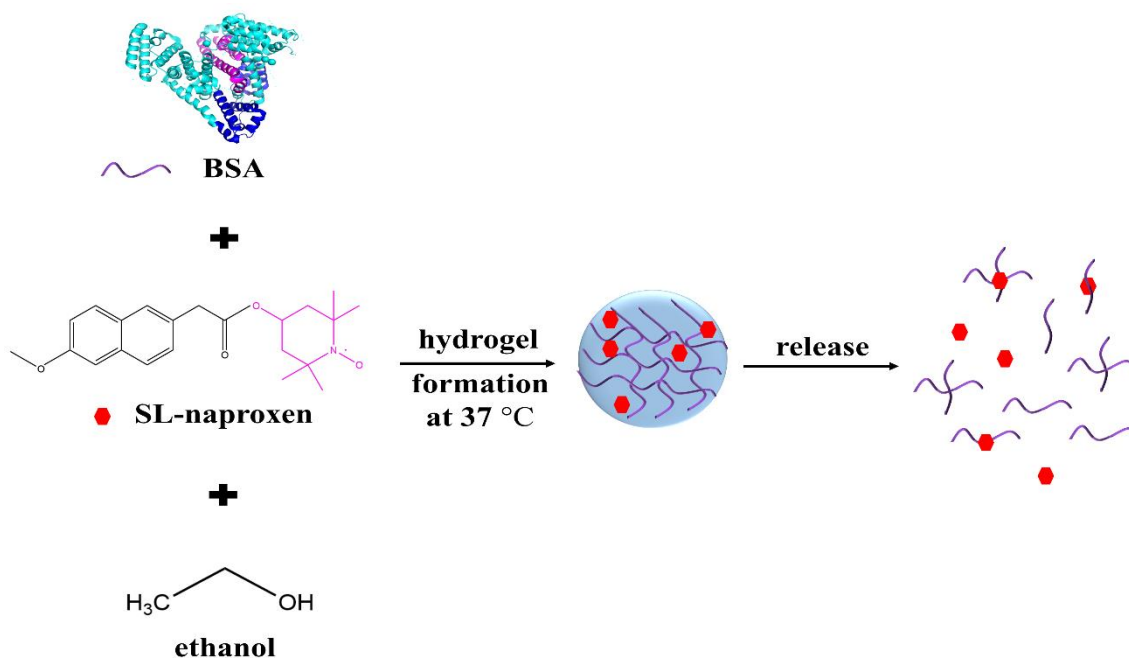


Figure 4.3 Schematic representation of SL-naproxen release from BSA hydrogels.

Patients with chronic inflammatory disorders require long treatment with naproxen, a nonsteroidal anti-inflammatory drug, which is commonly used to relieve fever and to treat osteoarthritis, bone pain, inflammation and headaches. However, this drug shows short bioavailability by oral administration, therefore, frequent dosing is required to maintain pharmacological action. Hence, it seems crucial to develop a controlled drug delivery system to reduce the frequency of administration and allow the sustained release of naproxen in order to increase

patient compliance [52, 74].

The objective of the present project was directed towards the development of a controlled drug delivery system that could be applied in local delivery based on BSA gels which were prepared by ethanol induced method at 37 °C, and study the release behavior of SL-NPX from the prepared hydrogels.

In the first chapter of this study, the effects of different volumes of ethanol and BSA concentrations on the mechanical and viscoelastic behavior of hydrogels were investigated and the results were compared with gels prepared by thermally and induced methods. The results suggested that it is possible to form hydrogels with different mechanical properties by tuning the ethanol concentrations. Furthermore, the addition of high amounts of ethanol allowed us to obtain hydrogels at 37 °C and neutral pH that were mechanically as tough as those formed by the other mentioned procedures. Moreover, the ethanol-induced changes in secondary structure of BSA at 37 °C were explored by means of ATR-IR spectroscopy, which demonstrated the important role of ethanol volume in gel formation.

In the second part of this project, the SL-NPX loaded hydrogels as well as the release behavior of this SL-pharmaceutical from ethanol-induced gels were characterized by EPR spectroscopy. EPR data indicated that ethanol induced hydrogels can lower SL-pharmaceutical binding capacity, resulting in weaker interaction between BSA and SL-NPX in comparison with gels formed by thermally and pH induced methods. Moreover, faster and higher release rate was obtained by the addition of lower amounts of ethanol, lower BSA concentration and higher drug loading ratios.

## **4.2 Publications**

In the following, the three published papers contributing to this thesis are presented.

**Nanoscopic characterization of stearic acid release from bovine serum albumin hydrogels**

Niuosha Sanaeifar, Karsten Mäder, and Dariush Hinderberger

Macromolecular Bioscience. 20(8), 2000126 (2020).

DOI: [\*\*10.1002/mabi.202000126\*\*](https://doi.org/10.1002/mabi.202000126)

**Molecular-level release of coumarin-3-carboxylic acid and warfarin-derivatives from BSA-based hydrogels**

Niuosha Sanaeifar, Karsten Mäder, and Dariush Hinderberger

Pharmaceutics. 13(10), 1661 (2021).

DOI: [\*\*10.3390/pharmaceutics13101661\*\*](https://doi.org/10.3390/pharmaceutics13101661)

**Macro- and nanoscale effect of ethanol on bovine serum albumin gelation and naproxen release**

Niuosha Sanaeifar, Karsten Mäder, and Dariush Hinderberger

International Journal of Molecular Sciences. 23(13), 7352 (2022).

DOI: [10.3390/ijms23137352](https://doi.org/10.3390/ijms23137352)



## 5 Discussion

The published papers presented in my thesis cover the macroscopic and nanoscopic properties of hydrogels made from BSA, and release behavior of a fatty acid and different SL-pharmaceuticals from these hydrogels prepared by different methods.

The focus of paper [P1] was laid on the nanoscopic characterization of 16-DSA release, which serves as an amphiphilic model drug, from BSA hydrogels prepared by thermally and pH induced procedures.

It is crucial to choose a preparation method for obtaining robust albumin hydrogels while maintaining different functions of albumin like its binding ability and release of various types of molecules. Moreover, mechanical and viscoelastic behavior of the hydrogel play a significant role, since the rigidity or flowability of the gel depends only on the hydrogel mechanical properties [27]. By heating the precursor solution of BSA above and below its denaturation temperature at 65 °C and 59 °C, respectively, it was possible to obtain mechanically robust hydrogels. It is important to mention that gelation started immediately for both hydrogels, however, the storage modulus of the gel prepared at 65 °C was much higher than the one prepared at 59 °C. The hydrogel prepared at 37 °C by lowering the pH to 3.5, required much longer incubation times to be mechanically tough, since there was no sign of gelation during the first 25 minutes and the value of storage modulus was considerably low. By adding different amounts of stearic acid (SA), which has been shown to be interchangeable with 16-DSA concerning its binding properties to BSA [38, 48], the potential effect of fatty acid on albumin gelation was studied. The results revealed that the addition of stearic acid slowed down gel formation and deeply impacted the mechanical properties. The concentration of SA determined the extent of reduction in mechanical strength.

As expected, the secondary structure of the protein underwent stronger changes during gelation when the temperature was above the denaturation temperature. ATR-IR spectroscopy provided information on the protein's secondary structure. The results from IR were comparable with the rheological characterization data, since the storage modulus value of the hydrogel formed at 65 °C was

considerably greater than the one prepared at 59 °C, suggesting that changes in the secondary structure content of the individual protein and mechanical strength of the hydrogel were correlated.

The main goal of this paper was to study the effects of fatty acid concentration, hydrogel incubation time (the time at which gelation is processing at specific temperature or pH), and gelation procedures on 16-DSA release behavior. The release curves for different samples in PBS buffer were analyzed by plotting the double integral of the EPR spectra against various time intervals. The results suggested that all hydrogels, regardless of fatty acid concentration, gel preparation methods and incubation time, showed an initial burst release during the first 24 hours, followed by a sustained release over later times. Furthermore, by observing the effect of initial 16-DSA loading on the release profile from different hydrogels, it was found that increase in the model drug contents led to a faster and higher release rate in all experimental systems.

The other important parameter to consider was the incubation time, which had direct impact on the release rate. Increasing the gelation time resulted in lower release rate due to the higher mechanical properties of the hydrogel networks. Therefore, it was possible to change the release rate by changing the fatty acid concentration, incubation time and preparation methods, which indicated the potential for tuning BSA hydrogels for drug delivery applications.

The relative percentages of tightly and intermediately bound 16-DSA to BSA and freely rotating 16-DSA, can be given by EPR spectral simulations. These results revealed that more freely tumbling and intermediately bound FAs were released from hydrogels with higher incubation time, while more strongly bound FAs were found in buffer medium for hydrogels with lower incubation times. As it was mentioned before, higher incubation times led to more rigid networks, in which less individual albumin molecules and aggregates can be released. However, shorter incubation times resulted in looser gel structures that allowed the release of BSA, in which FAs were transported.

The investigation of the nature of the components released over time suggested that size of the particles released from hydrogels prepared by pH induced method by lowering the pH to 3.5, were much larger than those released from thermally induced hydrogels. Moreover, all different hydrogels prepared by different procedures with lower incubation times showed the release of larger structures.

The larger components could be attributed to the release of strongly bound FAs to BSA, which are larger structures in comparison with free 16-DSA or 16-DSA intermediately bound to BSA.

In paper [P2], the release behavior of two SL-drugs, namely SL-CCS and SL-WFR from BSA hydrogels were investigated. We used the same preparation methods as in the previous paper, namely thermally and pH induced procedures for BSA gel formation. We aimed at studying the influence of the method of gel formation, the drug concentration, and the incubation time on the mechanical properties of the gels, the interaction and spatial distribution of SL-drugs with BSA gels, release behavior, and the size and nature of released components.

As it was discussed in the previous paper, the mechanical properties of hydrogels have direct effect on the release behavior. Therefore, it was vital to investigate the effect of mentioned drugs on hydrogels mechanical properties. The addition of different ratios of CCS and WFR to the precursor solutions of BSA led to some changes in the mechanical and viscoelastic behavior of the hydrogels. In hydrogels, prepared thermally at 65 °C, the addition of WFR/ CCS led to a lower storage modulus and mechanically weaker hydrogels compared to the BSA hydrogel formed at the same temperature without CCS or WFR. Presence of CCS or WFR in the Sudlow binding sites in albumin stabilized BSA structure to some extent and thus hindered the conformational changes. Furthermore, the rheological characterization revealed that the concentration of CCS or WFR could not deeply affect thermally-induced gelation, since the storage modulus values for different drug ratios were similar. However, pH induced hydrogels showed opposite behavior. When CCS was added to the BSA precursor solution, gelation started faster and the  $G'$  value increased slightly. Apparently, this preparation method did not allow CCS to fully bind to Sudlow sites and instead may interact with the surface of the protein, which may facilitate denaturation and then resulted in the earlier gelation starting point. The same behavior was observed by addition of WFR at WFR: BSA 0.5:1 and 1:1 molar ratios. Although, it seemed that by increasing the ratio to WFR: BSA 2:1 the storage modulus decreased. In general, as it was mentioned in paper [P1], thermally induced hydrogels with or without CCS and WFR were mechanically more robust than the same gel prepared by reducing the pH to 3.5.

The comparison of the results from EPR spectral simulation of hydrogels

prepared by thermally induced method with those prepared by pH induced procedure showed that addition of acid increased the percentage of freely rotating and intermediately immobilized SL-CCS, while that of the strongly bound ligand to BSA decreased. Moreover, the percentage of strongly immobilized and intermediately bound SL-WFR was higher in different hydrogels, prepared either by thermally or pH induced methods, than in SL-CCS loaded BSA. This was due to the difference in chemical substitution of both drugs. The free 3-oxo-1-phenylbutyl group in SL-WFR can provide flexibility to its coumarin backbone in a way that the 3-oxo group can facilitate hydrogen bonding in protein, therefore it can increase the average binding affinity. While, SL-CCS with no additional group has less flexibility and only the carbonyl group at position 2 may have a hydrogen-bond acceptor function (Figure 2.3).

The release profiles of SL-CCS loaded BSA hydrogels prepared by different methods at 0.5:1 and 1:1 molar ratios showed an initial fast release followed by a sustained release over the later time periods. In contrast, increasing the ratio to 2:1 resulted in zero-order release kinetics with an initial burst effect. The initial fast release was due to the diffusion of buffer medium into the protein network, which could dissolve the entrapped SL-CCS close to or at the surface of the hydrogel. However, slower and sustained release corresponded to the reduction of drug in the inner part of gel matrix, which resulted in the increase in the diffusion process length. A constant release rate in a sample with 2:1 SL-CCS:BSA molar ratio could be due to the fully occupied binding sites from which later release occurred, therefore the amount of drug between hydrogel networks increased, resulting in a zero-order drug release kinetics.

SL-WFR loaded BSA hydrogels showed an initial fast release for all of the ratios, and a later sustained release at the 0.5:1 SL-WFR:BSA molar ratio. The higher ratios of SL-WFR followed the zero order kinetics and reached the plateau after approximately 100 hours. We observed that all hydrogels with SL-CCS, regardless of molar ratios and preparation methods, had a higher release rate than SL-WFR loaded BSA gels, which may be attributed to the higher affinity of SL-WFR to albumin compared to SL-CCS.

In all experimental systems, increasing the concentration of SL-pharmaceuticals led to a higher release rate. Moreover, thermally induced hydrogels at 65 °C and 59 °C had higher release rates than pH-induced hydrogels. When comparing the

release rate from hydrogels prepared at 65 °C with the respective rate for the ones prepared at 59 °C, the results revealed that hydrogels prepared at 59 °C showed higher release rate.

Changing the incubation time had also a direct impact on the release profile, as increasing the incubation time led to a slight decrease in the rate of drug release. EPR spectral simulation of the release medium suggested that the percentage of released components in bound, intermediate, and free states was almost constant during the different release time intervals for all samples, while in the previous paper about fatty acid release, these percentages changed during the release experiment. Moreover, there was no sign of strongly bound SL-drugs (SL-WFR/ SL-CCS) to BSA for the samples prepared by thermally induced method at 65 °C. However, the percentage of tightly bound SL-drugs to BSA in the release medium increased when the hydrogels were prepared by pH-induced method.

Following the characterization of release profile, the spectral-spatial two-dimensional EPR image of SL-pharmaceuticals inside the slowly dissolving gels not in the release medium were studied. It was seen that the signal intensity decreased over time, which showed the release of the SL-drugs from hydrogels. Moreover, the hydrogel at a lowest SL-CCS: BSA molar ratio had the lowest amount of spin probe inside the gel due to the lowest initial drug content, while increasing the drug loading percentage led to a higher drug percentage in hydrogels over the whole release period.

DLS data revealed that smaller particles were released when hydrogels were prepared with higher incubation time, since these hydrogels were mechanically more robust. Therefore, smaller albumin derivatives formed during gelation process were released. In addition, the size of the components released from pH induced hydrogels were much larger than those released from thermally induced hydrogels.

The results of this research paper, support former evidence from paper [P1] that BSA hydrogels can be potentially exploited in controlled drug delivery applications.

In paper [P3], we investigated ethanol induced gelation method for BSA at 37 °C and studied the release behavior of SL-NPX from this hydrogel.

To gain insight into the mechanical properties of ethanol induced hydrogels, the

results of these hydrogels were compared with gels prepared by thermally and pH induced methods. The results showed that it is possible to form hydrogels with different mechanical properties by tuning the ethanol concentrations. Furthermore, the addition of high amounts of ethanol allowed us to obtain hydrogels at 37 °C and neutral pH, which were mechanically as strong as those formed by increasing the temperature to 59/65°C and lowering the pH to 3.5. However, it is important to note that visual evaluation showed that addition of extremely high amount of ethanol resulted in the immediate formation of large white BSA aggregates. Furthermore, we presented a correlation between BSA and ethanol concentrations. When the amount of ethanol was constant, increasing the concentration of BSA led to a more mechanically robust hydrogels. However, it was possible to obtain robust hydrogels by increasing the volume of ethanol even at low BSA concentrations.

Since mechanical properties have direct impact on the release profile, the effect of SL-NPX on ethanol induced gelation was studied. It seemed that addition of SL-NPX could enhance the viscoelastic behavior and led to a higher storage modulus. However, as it was discussed in the previous paper, addition of CCS and WFR to the BSA precursor solution could decrease the G' value of thermally induced hydrogels, but slightly strengthen the mechanical properties when the hydrogels were prepared by reducing pH.

The results of time-dependent ATR-IR measurements showed that despite high BSA concentration no significant changes in the secondary structure of protein could be observed when low amount of ethanol is added, indicating that no gel was formed under this condition. However, by increasing the amounts of ethanol,  $\alpha$ -helices and intramolecular  $\beta$ -sheets were converted to intermolecular  $\beta$ -sheets, which led to a three-dimensional network structure and gel formation. Moreover, the extent of conformational changes strongly depends on the ethanol concentration.

Using CW EPR spectroscopy, we found that presence of ethanol in solution and hydrogels could increase the percentage of freely tumbling drug, since ethanol can be considered as a good solvent for SL-NPX, so that this SL-pharmaceutical preferred ethanol solvation instead of BSA binding sites (which it would prefer in water). Comparing the ethanol induced hydrogels with those prepared by thermally and pH induced procedures showed that addition of high amounts of

ethanol led to a higher fraction of freely rotating SL-NPX. In other words, presence of ethanol could decrease the binding capacity of SL-drug which led to the weaker interaction between BSA and SL-NPX in comparison with other gel preparation methods.

The other parameters, which can affect the interaction of BSA with SL-NPX and the binding capacities of hydrogels, are incubation time and protein concentration. We found that increasing the incubation time and the amount of BSA led to the higher fraction of strongly bound components in the hydrogel.

The release profiles of SL-NPX from ethanol induced hydrogels revealed that increasing the amount of BSA precursor solution and that of ethanol resulted in significant decrease in drug release. According to rheological measurements and ATR spectroscopy, mechanically weak hydrogels could be obtained by lowering the concentration of ethanol and BSA, which allowed faster diffusion of drug from the gel into the release medium. The other significant parameters affecting the release rate were initial drug loading and incubation time. Increasing the concentration of SL-NPX in hydrogels prepared by the same conditions could result in the higher release rate. Moreover, increasing the incubation time of the hydrogels prepared with the same amount of BSA, ethanol and SL-NPX lowered the release rate due to the formation of a more robust hydrogel network.

Similar to the other two papers, the relative fractions of tightly and intermediately bound SL-drug and freely tumbling SL-NPX in the release medium were obtained by EPR spectral simulation. The results revealed that in the sample prepared by a low amount of ethanol, the highest percentage of released SL-NPX was attached intermediately to BSA, low percentage tumble freely and no strongly bound component was found within the first 24 hours of the release. However, the percentage of strongly bound SL-NPX to BSA increased over longer time periods later and those of the intermediately bound and freely rotating decreased sharply which was due to the mechanically weak structure of this hydrogel. However, when higher amount of ethanol was added or the incubation time was increased, the fraction of intermediately bound SL-NPX increased over release time and that of the freely rotating SL-NPX decreased. For such hydrogels, there was no sign of strongly bound SL-NPX, which was due to their strong mechanical properties, therefore less individual albumin molecules and albumin aggregates could be released.

Hydrogels prepared with lower amount of ethanol released larger structures, since these hydrogels were mechanically weak, which led to the release of larger albumin molecular aggregates formed during gelation. Furthermore, by keeping the amount of ethanol constant and increasing the incubation time or BSA concentration, smaller particles were released.

The results of this project showed the fine tuning capability of BSA hydrogels as controlled release systems due to the variety of gelation parameter.

Comparison of all papers presented in this thesis reveals several similarities. Rheological characterization as well as ATR-IR measurements, parallel to CW EPR spectroscopy provided macroscopic and nanoscopic properties of BSA hydrogels. CW EPR measurements and DLS enable investigation of release behavior from hydrogels. The results discussed before suggest some similar effects occurring in all release system. In all studies, increasing the drug/ fatty acid concentration led to a higher release rate, while increasing the incubation time resulted in lower rate of release from BSA hydrogels. Moreover, the release behavior can be controlled by changing various parameters, which shows the potential of BSA hydrogels as controlled drug delivery systems for implementation in pharmaceutical applications.



## 6 Conclusions and Outlook

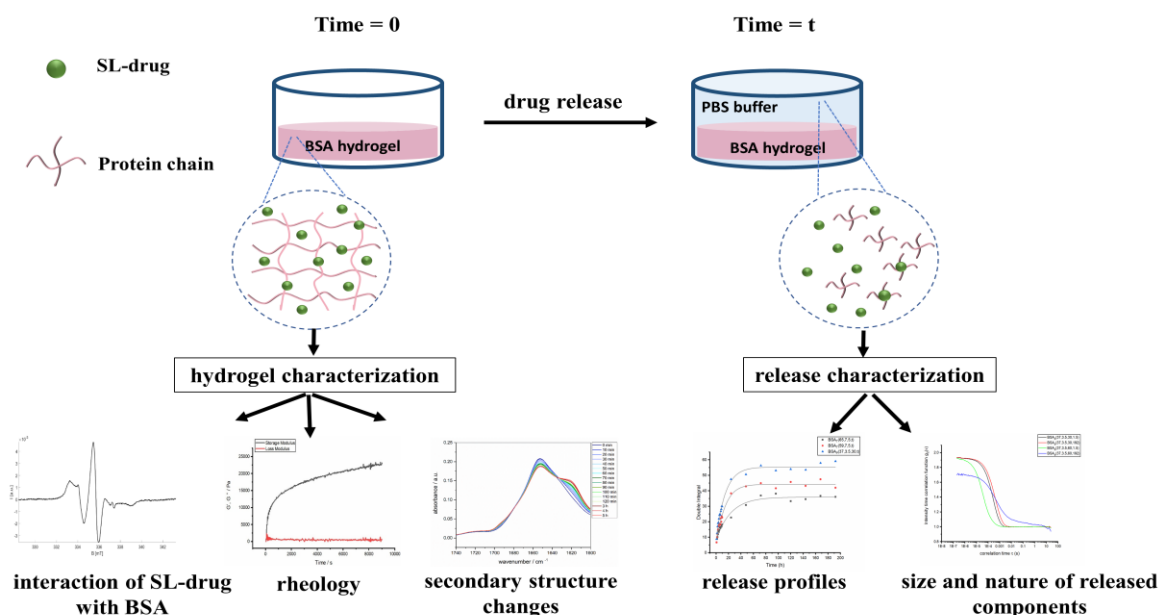


Figure 6.1 Graphical representation of the research done during the work for this thesis.

During the research in my doctorate, I developed controlled release systems based on BSA hydrogels to investigate the release behavior of a fatty acid and different SL-pharmaceuticals. The general approach used in this thesis is depicted graphically in Figure 6.1.

The nanoscopic characterization of stearic acid release from bovine serum albumin hydrogels in paper [P1] displayed the potential of BSA hydrogels as suitable candidates for controlled drug delivery applications. In this research, the applicability of the hydrogels prepared by thermally and pH induced procedures as delivery hosts was evaluated by loading different molar ratios of 16-DSA as a model drug into these structures. It was shown that parameters such as 16-DSA concentration, incubation time and gelation method can deeply affect the release rate. Higher fatty acid ratios, lower incubation times and gel formation below the protein denaturation temperature led to higher initial and later sustained release rates. However, all release profiles from different hydrogels regardless of the mentioned parameters displayed initial fast release during the first 24 hours followed by the sustained release over later time periods. Moreover, we were able to study the interaction of 16-DSA with BSA and monitor the size and nature of released components.

The second project presented here deals with the release of SL-CCS and SL-WFR from BSA hydrogels prepared by the same methods as described in paper [P1] in detail. The main objective of this work was to prepare BSA hydrogels as delivery hosts to investigate and compare the release behavior of SL-CCS and SL-WFR. Similar to the previous published paper, the results suggested that the release rate depends on SL-drug concentration, incubation time, and gelation methods. It has been found that SL-CCS had much higher release rate than SL-WFR. The release pattern from different hydrogels revealed that they can be used where the initial burst release is required. Furthermore, we found that release behavior can be tuned by initial drug loading. In other words, at lower drug ratios the release profile showed the second sustained release phase, while a zero-order kinetics can be obtained at higher ratios.

Additionally, the interaction of drug with BSA can be deeply affected due to differences in chemical substitutions of the two SL-pharmaceuticals. Higher percentage of SL-WFR was bound strongly and intermediately to BSA due to higher affinity to the binding sites of this protein, therefore, higher percentage of these structures were released in comparison with the SL-CCS loaded BSA, in which more of the freely tumbling SL-drug was found in release medium.

Paper [P3] presents a macro- and nanoscale effect of ethanol on BSA gelation and naproxen release. The main focus of this work was to develop ethanol-induced hydrogels as delivery systems for controlled and potentially local drug delivery applications. These hydrogels were used to investigate the release behavior of the SL-NPX. We found that ethanol and BSA concentrations have direct impact on mechanical properties of hydrogels and thus the release rate. In general, lower BSA and ethanol concentrations resulted in higher release rate. However, there was a low limit concentration, below which gel networks cannot form. The release profiles from hydrogels prepared with different ethanol and BSA concentrations showed an initial burst release during early times followed by a sustained release over later times.

In conclusion, this thesis contributes to several research fields including preparing hydrogels from BSA with different methods, namely thermally, pH and ethanol induced procedures, characterization of mechanical and viscoelastic properties of these hydrogels, studying changes in the secondary structure of protein during gelation, loading different SL-pharmaceuticals and a fatty acid into

hydrogels to investigate the release behavior of the drugs, the interaction of SL-drugs with BSA and size and nature of released components, as is presented schematically in Figure 6.1. The results gathered during this dissertation highlight the importance of understanding the properties of the system of interest. Although many aspects of controlled drug delivery system have been elucidated in previous sections, each result evokes new questions that this thesis cannot fully cover. Therefore further research is required to obtain more insight into this topic.

## 7 References

1. Zhang, A., et al., *Recent advances in stimuli-responsive polymer systems for remotely controlled drug release*. Progress in Polymer Science, 2019. **99**: p. 101164.
2. Iqbal, Z., A. Babar, and M. Ashraf, *Controlled-release naproxen using micronized ethyl cellulose by wet-granulation and solid-dispersion method*. Drug development and industrial pharmacy, 2002. **28**(2): p. 129-134.
3. Safdar, R., et al., *Potential of Chitosan and its derivatives for controlled drug release applications—A review*. Journal of drug delivery science and technology, 2019. **49**: p. 642-659.
4. Dash, S., et al., *Kinetic modeling on drug release from controlled drug delivery systems*. Acta Pol Pharm, 2010. **67**(3): p. 217-23.
5. Zaghloul, A.A., et al., *Response surface methodology to obtain naproxen controlled release tablets from its microspheres with Eudragit L100-55*. Journal of microencapsulation, 2001. **18**(5): p. 651-662.
6. Iemma, F., et al., *pH-sensitive hydrogels based on bovine serum albumin for oral drug delivery*. International journal of pharmaceutics, 2006. **312**(1-2): p. 151-157.
7. Al-Kady, A.S., et al., *Nanostructure-loaded mesoporous silica for controlled release of coumarin derivatives: a novel testing of the hyperthermia effect*. European journal of pharmaceutics and biopharmaceutics, 2011. **77**(1): p. 66-74.
8. Bhowmik, D., et al., *Controlled release drug delivery systems*. The Pharma Innovation, 2012. **1**(10).
9. Shen, J. and D.J. Burgess, *Accelerated in-vitro release testing methods for extended-release parenteral dosage forms*. Journal of Pharmacy and Pharmacology, 2012. **64**(7): p. 986-996.
10. Cao, Z., et al., *ROS-sensitive polymeric nanocarriers with red light-activated size shrinkage for remotely controlled drug release*. Chemistry of Materials, 2018. **30**(2): p. 517-525.
11. Thanh, V.M., et al., *Low systemic toxicity nanocarriers fabricated from heparin-mPEG and PAMAM dendrimers for controlled drug release*. Materials Science and Engineering: C, 2018. **82**: p. 291-298.
12. de Souza, L.E., et al., *Has PEG-PLGA advantages for the delivery of hydrophobic drugs? Risperidone as an example*. Journal of Drug Delivery Science and Technology, 2021. **61**: p. 102239.
13. Janich, C., et al., *Risperidone-Loaded PLGA–Lipid Particles with Improved Release Kinetics: Manufacturing and Detailed Characterization by Electron Microscopy and Nano-CT*. Pharmaceutics, 2019. **11**(12): p. 665.

14. Wells, C.M., et al., *Stimuli-responsive drug release from smart polymers*. Journal of functional biomaterials, 2019. **10**(3): p. 34.
15. Xiong, D., et al., *Smart pH-sensitive micelles based on redox degradable polymers as DOX/GNPs carriers for controlled drug release and CT imaging*. Colloids and Surfaces B: Biointerfaces, 2018. **163**: p. 29-40.
16. Lai, W., et al., *Hydrothermal fabrication of porous hollow hydroxyapatite microspheres for a drug delivery system*. Materials Science and Engineering: C, 2016. **62**: p. 166-172.
17. Sharma, P.K., S. Taneja, and Y. Singh, *Hydrazone-linkage-based self-healing and injectable xanthan–poly (ethylene glycol) hydrogels for controlled drug release and 3D cell culture*. ACS applied materials & interfaces, 2018. **10**(37): p. 30936-30945.
18. Wang, Y., et al., *Chitosan cross-linked poly (acrylic acid) hydrogels: drug release control and mechanism*. Colloids and Surfaces B: Biointerfaces, 2017. **152**: p. 252-259.
19. Caccavo, D., et al., *Controlled drug release from hydrogel-based matrices: Experiments and modeling*. International journal of pharmaceutics, 2015. **486**(1-2): p. 144-152.
20. Sanaeifar, N., K. Mäder, and D. Hinderberger, *Molecular-Level Release of Coumarin-3-Carboxylic Acid and Warfarin-Derivatives from BSA-Based Hydrogels*. Pharmaceutics, 2021. **13**(10): p. 1661.
21. Li, J. and D.J. Mooney, *Designing hydrogels for controlled drug delivery*. Nature Reviews Materials, 2016. **1**(12): p. 1-17.
22. Langer, R. and N.A. Peppas, *Advances in biomaterials, drug delivery, and bionanotechnology*. AIChE Journal, 2003. **49**(12): p. 2990-3006.
23. Ghasemiyeh, P. and S. Mohammadi-Samani, *Hydrogels as drug delivery systems; pros and cons*. Trends in Pharmaceutical Sciences, 2019. **5**(1): p. 7-24.
24. Lee, P. and X. Wu, *Modifications of human serum albumin and their binding effect*. Current pharmaceutical design, 2015. **21**(14): p. 1862-1865.
25. Khodarahmi, R., et al., *Comparative spectroscopic studies on drug binding characteristics and protein surface hydrophobicity of native and modified forms of bovine serum albumin: possible relevance to change in protein structure/function upon non-enzymatic glycation*. Spectrochimica Acta Part A: Molecular and Biomolecular Spectroscopy, 2012. **89**: p. 177-186.
26. Tantra, R., J. Tompkins, and P. Quincey, *Characterisation of the de-agglomeration effects of bovine serum albumin on nanoparticles in aqueous suspension*. Colloids and Surfaces B: Biointerfaces, 2010. **75**(1): p. 275-281.
27. Sanaeifar, N., K. Mäder, and D. Hinderberger, *Nanosopic Characterization of Stearic Acid Release from Bovine Serum Albumin Hydrogels*. Macromolecular bioscience, 2020. **20**(8): p. 2000126.

28. Larsen, M.T., et al., *Albumin-based drug delivery: harnessing nature to cure disease*. Mol Cell Ther, 2016. **4**: p. 3.
29. Joshi, R., et al., *Is the Sudlow site I of human serum albumin more generous to adopt prospective anti-cancer bioorganic compound than that of bovine: A combined spectroscopic and docking simulation approach*. Bioorganic Chemistry, 2017. **75**: p. 332-346.
30. van der Vusse, G.J., *Albumin as fatty acid transporter*. Drug metabolism and pharmacokinetics, 2009. **24**(4): p. 300-307.
31. Murayama, K. and M. Tomida, *Heat-Induced Secondary Structure and Conformation Change of Bovine Serum Albumin Investigated by Fourier Transform Infrared Spectroscopy*. Biochemistry, 2004. **43**(36): p. 11526-11532.
32. Borzova, V.A., et al., *Kinetics of thermal denaturation and aggregation of bovine serum albumin*. PloS one, 2016. **11**(4): p. e0153495.
33. Tada, D., et al., *Drug release from hydrogel containing albumin as crosslinker*. Journal of bioscience and bioengineering, 2005. **100**(5): p. 551-555.
34. Boye, J.I., I. Alli, and A.A. Ismail, *Interactions involved in the gelation of bovine serum albumin*. Journal of Agricultural and Food Chemistry, 1996. **44**(4): p. 996-1004.
35. Baler, K., et al., *Albumin hydrogels formed by electrostatically triggered self-assembly and their drug delivery capability*. Biomacromolecules, 2014. **15**(10): p. 3625-3633.
36. Ong, J., et al., *Albumin-based hydrogels for regenerative engineering and cell transplantation*. Biotechnology and bioengineering, 2019. **116**(12): p. 3457-3468.
37. Vesković, A., Đ. Nakarada, and A.P. Bijelić, *A novel methodology for hydrogel water content determination by EPR: The basis for real-time monitoring of controlled drug release and hydrogel swelling and degradation*. Polymer Testing, 2021. **98**: p. 107187.
38. Arabi, S.H., et al., *Serum albumin hydrogels in broad pH and temperature ranges: characterization of their self-assembled structures and nanoscopic and macroscopic properties*. Biomaterials science, 2018. **6**(3): p. 478-492.
39. Wagner, J., et al., *Effect of ethanol on the microstructure and rheological properties of whey proteins: Acid-induced cold gelation*. LWT, 2021. **139**: p. 110518.
40. Wagner, J., C.G. Biliaderis, and T. Moschakis, *Whey proteins: Musings on denaturation, aggregate formation and gelation*. Critical reviews in food science and nutrition, 2020. **60**(22): p. 3793-3806.
41. Elysée-Collen, B. and R.W. Lencki, *Effect of ethanol, ammonium sulfate, fatty acids, and temperature on the solution behavior of bovine serum albumin*. Biotechnology progress, 1997. **13**(6): p. 849-856.

42. Lurie, D.J. and K. Mäder, *Monitoring drug delivery processes by EPR and related techniques—principles and applications*. *Advanced drug delivery reviews*, 2005. **57**(8): p. 1171-1190.
43. Akdogan, Y., et al., *EPR studies of intermolecular interactions and competitive binding of drugs in a drug–BSA binding model*. *Physical Chemistry Chemical Physics*, 2016. **18**(32): p. 22531-22539.
44. Martini, G. and L. Ciani, *Electron spin resonance spectroscopy in drug delivery*. *Physical Chemistry Chemical Physics*, 2009. **11**(2): p. 211-254.
45. Mäder, K., et al., *Monitoring microviscosity and microacidity of the albumin microenvironment inside degrading microparticles from poly (lactide-co-glycolide)(PLG) or ABA-triblock polymers containing hydrophobic poly (lactide-co-glycolide) A blocks and hydrophilic poly (ethyleneoxide) B blocks*. *Pharmaceutical research*, 1998. **15**(5): p. 787-793.
46. Besheer, A., et al., *Loading and mobility of spin-labeled insulin in physiologically responsive complexation hydrogels intended for oral administration*. *Journal of controlled release*, 2006. **111**(1-2): p. 73-80.
47. Kempe, S., H. Metz, and K. Mäder, *Application of electron paramagnetic resonance (EPR) spectroscopy and imaging in drug delivery research—chances and challenges*. *European Journal of Pharmaceutics and Biopharmaceutics*, 2010. **74**(1): p. 55-66.
48. Reichenwallner, J. and D. Hinderberger, *Using bound fatty acids to disclose the functional structure of serum albumin*. *Biochimica et Biophysica Acta (BBA)-General Subjects*, 2013. **1830**(12): p. 5382-5393.
49. Msolli, I., et al., *Synthesis of nanoparticles based on PDMMLA derivative copolymers and study of warfarin encapsulation and controlled release*. *RSC advances*, 2017. **7**(11): p. 6704-6711.
50. Khalil, S.K., et al., *Preparation and evaluation of warfarin- $\beta$ -cyclodextrin loaded chitosan nanoparticles for transdermal delivery*. *Carbohydrate polymers*, 2012. **90**(3): p. 1244-1253.
51. Ilić-Stojanović, S., et al., *Semi-Crystalline copolymer hydrogels as smart drug carriers: in vitro thermo-responsive naproxen release study*. *Pharmaceutics*, 2021. **13**(2): p. 158.
52. Şanlı, O. and E.K. Solak, *Controlled release of naproxen from sodium alginate and poly (vinyl alcohol)/sodium alginate blend beads crosslinked with glutaraldehyde*. *Journal of applied polymer science*, 2009. **112**(4): p. 2057-2065.
53. Wiki, A.P., *Basics of rheology*. 2018, Dostopno na: <https://wiki.antonpaar.com/en/basics-of-rheology> ...
54. Arabi, S.H., D. Haselberger, and D. Hinderberger, *The effect of ethanol on gelation, nanoscopic, and macroscopic properties of serum albumin hydrogels*. *Molecules*, 2020. **25**(8): p. 1927.
55. Barbucci, R., et al., *Synthesis, chemical and rheological characterization of new hyaluronic acid-based hydrogels*. *Journal of Biomaterials Science, Polymer Edition*, 2000. **11**(4): p. 383-399.

56. Barnes, H.A., J.F. Hutton, and K. Walters, *An introduction to rheology*. Vol. 3. 1989: Elsevier.
57. Aboul-Enein, Y., A. Bunaciu, and S. Fleschin, *Evaluation of the protein secondary structures using Fourier Transform Infrared Spectroscopy*. Gazi University Journal of Science, 2014. **27**(1): p. 637-644.
58. Yang, H., et al., *Obtaining information about protein secondary structures in aqueous solution using Fourier transform IR spectroscopy*. Nature Protocols, 2015. **10**: p. 382.
59. Smith, B.C., *Fundamentals of Fourier transform infrared spectroscopy*. 2011: CRC press.
60. Fahrenfort, J., *Attenuated total reflection: A new principle for the production of useful infra-red reflection spectra of organic compounds*. Spectrochimica Acta, 1961. **17**(7): p. 698-709.
61. Huck, C., *Infrared spectroscopic technologies for the quality control of herbal medicines*, in *Evidence-Based Validation of Herbal Medicine*. 2015, Elsevier. p. 477-493.
62. Eisermann, J., *Colloid-like ionic clusters: structure formation with small molecules through weak interactions in solution*. 2019.
63. Bendix, J., *Electron Paramagnetic Resonance*. By Victor Chechik, Emma Carter, and Damien Murphy. 2017, Wiley Online Library.
64. Widder, K., *Characterisation of the effects of intrinsically disordered protein (IDP)-solvent and IDP-lipid interactions in aqueous solution and lipid monolayers*. 2019.
65. Van Doorslaer, S. and G. Jeschke, *Dynamics by EPR: picosecond to microsecond time scales*. Fluxional Organometallic and Coordination Compounds: p. 6-219.
66. Hruszowiec, M., et al., *The Microwave Sources for EPR Spectroscopy*. Journal of Telecommunications and Information Technology, 2017.
67. Stetefeld, J., S.A. McKenna, and T.R. Patel, *Dynamic light scattering: a practical guide and applications in biomedical sciences*. Biophysical reviews, 2016. **8**(4): p. 409-427.
68. Bhattacharjee, S., *DLS and zeta potential—what they are and what they are not?* Journal of controlled release, 2016. **235**: p. 337-351.
69. Goldberg, W.I., *Dynamic light scattering*. American Journal of Physics, 1999. **67**(12): p. 1152-1160.
70. Instruments, M., *Dynamic light scattering: an introduction in 30 minutes*. Technical Note Malvern, MRK656-01, 2012. **1**.
71. Berne, B.J. and R. Pecora, *Dynamic light scattering: with applications to chemistry, biology, and physics*. 2000: Courier Corporation.
72. Pereira, A.S., P. Tavares, and P. Limão-Vieira, *Radiation in Bioanalysis: Spectroscopic Techniques and Theoretical Methods*. 2019: Springer.
73. Elsadek, B. and F. Kratz, *Impact of albumin on drug delivery — New applications on the horizon*. Journal of Controlled Release, 2012. **157**(1): p. 4-28.



74. Mello, V.A.d. and E. Ricci-Júnior, *Encapsulation of naproxen in nanostructured system: structural characterization and in vitro release studies*. Química Nova, 2011. **34**: p. 933-939.

## 8 List of Abbreviations and Symbols

### 8.1 Abbreviations

16-DSA	16-doxy stearic acid
ATR-IR	Attenuated total reflection (ATR) Fourier transform infrared
BSA	bovine serum albumin
CCS	coumarin-3-carboxylic acid
CW EPR	continuous wave electron paramagnetic resonance
Cys	cysteine
DLS	dynamic light scattering
DMSO	dimethyl sulfoxide
EPRI	electron paramagnetic resonance imaging
EZ	electron Zeeman
FA	fatty acid
HCl	hydrochloric acid
HF	hyperfine interaction
HSA	human serum albumin
IR	infrared
MEC	minimum effective concentration
MTC	minimum toxic concentration
NMR	nuclear magnetic resonance
NPX	naproxen
NSAID	non-steroidal anti-inflammatory drugs
NZ	nuclear Zeeman
PBS	phosphate buffer saline
PLA	polylactic acid
PLGA	poly(lactic-co-glycolic acid)
HA	hydroxyapatite
SA	stearic acid
SEM	scanning electron microscopy
SL	spin-labeled
SLP	spin-labeled pharmaceuticals
WFR	warfarin

## 8.2 Symbols

$B_0$	strength of the applied magnetic field
$D_\tau$	diffusion coefficient
$D_\tau$	diffusion coefficient
$K_B$	Boltzmann coefficient
$R_h$	hydrodynamic radius
$\mu_B$	Bohr magneton
$\mu_N$	nuclear magneton
$\Delta E$	energy difference
A	shear area
D	diffusion tensor
E	ethanol induced method
F	shear force
$G'$	storage modulus
$G''$	loss modulus
$h$	Planck's constant
h	shear gap
I	intensity
/	spin of nucleus
$m_s$	magnetic quantum number
$n_c$	refractive index of crystal
$n_s$	refractive index of sample
P	pH induced method
s	deflection path
<b>S</b>	spin angular momentum
T	incubation time
T	thermally induced method
$\alpha$	hyperfine splitting constant
$\alpha_{iso}$	isotropic $^{14}\text{N}$ -hyperfine coupling constant
$\theta_c$	critical angle
$\theta_i$	angle of incidence
$\theta_R$	angle of refraction
$T$	absolute temperature

$g$	$g$ factor
$\gamma$	deformation
$\gamma_A$	strain amplitude
$\delta$	phase shift angle
$\eta$	viscosity
$\tau$	shear stress
$\tau_A$	stress amplitude
$\tau_c$	rotational correlation time
$\nu$	frequency of electromagnetic radiation

## 9 Acknowledgments

I would like to express my immense gratitude to my supervisor Prof. Dr. Dariush Hinderberger for providing the opportunity to pursue the work presented here, and his kindness, generative hints and support during my PhD. I would like to thank him for giving me the scientific freedom which motivates me even more throughout these years. I want to extend my thanks for his concern and guidance, which helped me to overcome all the obstacles I faced.

Moreover, I would like to thank Prof. Dr. Karsten Mäder for being the second supervisor of this dissertation.

Sincere thanks to the all current and former members of Prof. Hinderberger's working group, especially, Dr. Jana Eisermann, Dr. Jörg Reichenwallner, Dr. Haleh Haeri and Dr. Christian Schwieger for their support and numerous inspiring discussions. I also want to thank Jonas Volmer, Florian Lehman, Dr. Martin Kordts and other colleagues for helping me in every possible way and making a wonderful working environment.

Gratitude also goes to Heike Schimm and Annekatriin Rother for their great technical support.

I want to thank all reviewers for investing time in reading my thesis.

Furthermore, special thanks to my family for their endless support. Thank you a lot for being always there for me during hard times and standing beside me in my distress. I really appreciate your patience and kindness.

At last I thank the graduate school AgriPoly which is funded by European Social Funds (ESF) and the State of Saxony-Anhalt for supporting my research with their financial support.

# 10 Academic Curriculum Vitae

## Personal Data

Name                      Niuosha Sanaeifar

## Educational History

### Ph.D. in Physical Chemistry

Martin-Luther University Halle-Wittenberg  
Supervisor: Prof. Dr. Dariush Hinderberger  
Halle, Germany | 2018-2022

- Thesis title: Serum albumin hydrogels: Mechanically and chemically robust protein gels for drug delivery

### M.Sc. Biomedical Engineering-Biomaterials

Amirkabir University of Technology  
Tehran, Iran | 2014-2016

- Thesis title: Design and fabrication of nanobiosensor based on  $\text{Fe}_3\text{O}_4$  nanoparticles by using electrochemical method for glucose detection
- Overall GPA: 1.1 | MSc thesis: 1.0

### B.Sc. Biomedical Engineering-Biomaterials

Science and Research Branch Islamic Azad University  
Tehran, Iran | 2009-2013

- Thesis title: Fabrication of porous polyurethane scaffold and study of freezing temperature gradient
- Overall GPA: 1.6 | BSc thesis: 1.0

## Awards

- Full Scholarship (2018-2022): International Graduate School "Functional Polymers" (AGRIPOLY)
- MSc Project Sponsorship (2016): Iran Nanotechnology Innovation Council

## Publications

- Sanaeifar, N., K. Mäder, and D. Hinderberger, *Macro- and Nanoscale Effect of Ethanol on Bovine Serum Albumin Gelation and Naproxen Release*. International Journal of Molecular Sciences, **2022**. 23(13): p. 7352.
- Sanaeifar, N., K. Mäder, and D. Hinderberger, *Molecular-Level Release of Coumarin-3-Carboxylic Acid and Warfarin-Derivatives from BSA-Based Hydrogels*. Pharmaceutics, **2021**. 13(10): p. 1661.
- Sanaeifar, N., K. Mäder, and D. Hinderberger, *Nanoscopic Characterization of Stearic Acid Release from Bovine Serum Albumin Hydrogels*. Macromolecular bioscience, **2020**. 20(8): p. 2000126.
- Sanaeifar, N., et al., *A novel electrochemical biosensor based on Fe<sub>3</sub>O<sub>4</sub> nanoparticles-polyvinyl alcohol composite for sensitive detection of glucose*. Analytical Biochemistry, **2017**. 519: p. 19-26.

Halle (Saale), 30 June 2022